Annals of Botany **126**: 39–59, 2020
doi: 10.1093/aob/mcz190, available online at www.academic.oup.com/aob

ANNALS OF BOTANY
Founded 1887

Seed coat development in explosively dispersed seeds of *Cardamine hirsuta*

Ulla Neumann and Angela Hay*

Max Planck Institute for Plant Breeding Research, Carl-von-Linné-Weg 10, D-50829 Köln, Germany
** For correspondence. E-mail hay@mpipz.mpg.de*

Received: 5 July 2019 Returned for revision: 11 October 2019 Editorial decision: 19 November 2019 Accepted: 22 November 2019
Electronically published: 4 December 2019

• **Background and Aims** Seeds are dispersed by explosive coiling of the fruit valves in *Cardamine hirsuta*. This rapid coiling launches the small seeds on ballistic trajectories to spread over a 2 m radius around the parent plant. The seed surface interacts with both the coiling fruit valve during launch and subsequently with the air during flight. We aim to identify features of the seed surface that may contribute to these interactions by characterizing seed coat differentiation.
• **Methods** Differentiation of the outermost seed coat layers from the outer integuments of the ovule involves dramatic cellular changes that we characterize in detail at the light and electron microscopical level including immunofluorescence and immunogold labelling.
• **Key Results** We found that the two outer integument (oi) layers of the seed coat contributed differently to the topography of the seed surface in the explosively dispersed seeds of *C. hirsuta* vs. the related species *Arabidopsis thaliana* where seed dispersal is non-explosive. The surface of *A. thaliana* seeds is shaped by the columella and the anticlinal cell walls of the epidermal oi2 layer. In contrast, the surface of *C. hirsuta* seeds is shaped by a network of prominent ridges formed by the anticlinal walls of asymmetrically thickened cells of the sub-epidermal oi1 layer, especially at the seed margin. Both the oi2 and oi1 cell layers in *C. hirsuta* seeds are characterized by specialized, pectin-rich cell walls that are deposited asymmetrically in the cell.
• **Conclusions** The two outermost seed coat layers in *C. hirsuta* have distinct properties: the sub-epidermal oi1 layer determines the topography of the seed surface, while the epidermal oi2 layer accumulates mucilage. These properties are influenced by polar deposition of distinct pectin polysaccharides in the cell wall. Although the ridged seed surface formed by oi1 cell walls is associated with ballistic dispersal in *C. hirsuta*, it is not restricted to explosively dispersed seeds in the Brassicaceae.

Key Words: *Cardamine hirsuta*, *Arabidopsis thaliana*, explosive seed dispersal, seed coat, cell wall, pectin.

INTRODUCTION

Explosive seed dispersal is found in various flowering plants, from trees such as the dynamite tree *Hura crepitans* (Swaine and Beer, 1977; Vogel, 2005), to weeds such as the popping cress *Cardamine hirsuta* (Vaughn *et al*., 2011; Hofhuis *et al*., 2016). Explosive fracture of the fruit tissues in these plants converts stored elastic energy to kinetic energy to launch their seeds (Galstyan and Hay, 2018). However, it is difficult to identify the cellular and genetic processes that underpin such rapid movements. A key problem is that traits such as explosive seed dispersal are not found in a model species like *Arabidopsis thaliana* where the experimental tools for functional studies exist. To address this problem, genetic tools have been developed in the related species *C. hirsuta* to study the origin of traits, such as explosive seed dispersal, that are not present in *A. thaliana* (Hay and Tsiantis, 2016). While recent studies have addressed the cellular basis of explosive seed dispersal in *C. hirsuta* fruit (Hofhuis *et al*., 2016), less is known about the characteristics that distinguish its explosively dispersed seeds.

During seed launch, the surface of the seed transiently adheres to the coiling fruit valve in *C. hirstua* (Hofhuis *et al*., 2016). Various hypotheses for seed launch were explored and it was found that modelling a viscoelastic adhesion between seed and valve provided the best fit to seed launch velocities calculated from high speed movies (Hofhuis *et al*., 2016). In contrast to *C. hirsuta*, explosive dispersal in another *Cardamine* species, *C. parviflora*, is reported to be unreliable, as the majority of seeds fail to launch effectively (Hayashi *et al*., 2010). The mechanism of transient adhesion between seed and fruit valve was proposed to be the source of this unreliability (Hayashi *et al*., 2010). Therefore, interactions between the seed surface and the coiling fruit valve play an important role in determining effective seed launch.

Explosive dispersal launches seeds on ballistic trajectories. From a mechanics perspective, a large size, high density and compact shape of the seed is preferable for ballistic motion (Vogel, 2005). Comparing seeds from the related species *C. hirsuta* and *A. thaliana* showed that explosively dispersed seeds of *C. hirsuta* are more than five times larger and seven times heavier than *A. thaliana* seeds, which are dispersed non-explosively (Hay *et al*., 2014). Therefore, *C. hirsuta* seeds may be better suited to ballistic flight than *A. thaliana* seeds. The large contribution of drag to ballistic seed flight in *C. hirsuta* was evident in the sensitivity of modelled seed distributions to drag (Hofhuis *et al*., 2016). Simulations where the drag coefficient was reduced by 30 % resulted in seeds landing 0.3 m further away from the plant (Hofhuis *et al*.,

2016). Therefore, seed aerodynamics, including surface–air interactions, may contribute to the distribution of ballistically dispersed seeds.

A comparison of differentially expressed genes during the development of explosive *C. hirsuta* fruit and non-explosive *A. thaliana* fruit identified a significant enrichment of Gene Ontology terms related to cell wall remodelling (Gan *et al*., 2016). These genes encoded pectin methylesterases (PMEs), which are secreted by plant cells into the wall space where they remove protective methyl ester groups from pectin polysaccharides, and PME inhibitor (PMEI) proteins, which inhibit PME activity. The degree and pattern of pectin methyl esterification are predicted to strongly influence the mechanical and biochemical properties of cell walls (Cosgrove, 2016). Several *PMEI* genes were specifically expressed in *C. hirsuta* seeds and highly upregulated during fruit development (Gan *et al*., 2016). As expected, this high *PMEI* gene expression in *C. hirsuta* seeds was associated with lower PME enzymatic activity per unit protein in *C. hirsuta* than in *A. thaliana* seeds (Gan *et al*., 2016). Furthermore, *C. hirsuta* seeds accumulated pectin with a high degree of methyl esterification in asymmetrically thickened cell walls in the sub-epidermal seed coat layer (Gan *et al*., 2016). This thick cell wall distinguishes the seed coat of *C. hirsuta* and *A. thaliana* seeds. How these asymmetric cell wall thickenings differentiate during seed coat development and how they influence the surface structure of *C. hirsuta* seeds are open questions.

Development of the *A. thaliana* seed coat has been well studied (Beeckman *et al*., 2000; Haughn and Chaudhury, 2005), though most attention has focused on mucilage secretion in the outer epidermal cell layer (Haughn and Western, 2012) and flavonoid synthesis in the innermost cell layer (endothelium) (Lepiniec *et al*., 2006). Less attention has been paid to the sub-epidermal cell layer of the seed coat. However, this cell layer has been proposed to be mechanically sensitive in *A. thaliana* (Creff *et al*., 2015). According to this scenario, the sub-epidermal cell layer of the seed coat senses mechanical stresses exerted by the expanding endosperm and responds by thickening the cell wall adjacent to this stress (Creff *et al*., 2015). Unlike small *A. thaliana* seeds that grow within the open space of the two fruit locules, growth of the larger *C. hirsuta* seeds is constrained by available space in the locules. So, seeds grow in physical contact with adjacent fruit tissues throughout much of their development (Hofhuis *et al*., 2016). For this reason, mechanical stresses are likely to be exerted on the developing seed coat of *C. hirsuta* seeds from not only internal but also external tissues. Given these very different constraints on seed growth, it is unclear whether cell wall thickening in the *C. hirsuta* seed coat is a comparable mechanoresponse to that in *A. thaliana*.

Both *C. hirsuta* and *A. thaliana* have dehiscent siliques and disperse their seeds by pod shatter. In *A. thaliana*, pod shatter occurs in the dry fruit, after dehiscence has separated the valves from the replum to expose the seeds (Dinneny and Yanofsky, 2005). At this point, any external stimulus can cause the fruit structure to fall to pieces, termed ‘pod shatter’, and disperse the seeds. In comparison, seeds are dispersed by explosive pod shatter before the fruit dries in *C. hirsuta*. Valves acquire the competence to rapidly coil while green and turgid (Hofhuis *et al*., 2016). Therefore, seeds are dispersed at a much earlier stage of fruit development in *C. hirsuta* than in *A. thaliana*. This raises questions about how embryo and seed coat development is co-ordinated with fruit development in *C. hirsuta* to ensure that dispersed seeds are fully mature.

The seed coat protects the embryo against stresses in the external environment, and influences seed dormancy, germination and longevity. Given that seed development culminates in death of the seed coat cells, it is the metabolites, such as flavonoids, synthesized during seed coat differentiation that impart these protective functions to the seed coat. Flavonoids are plant secondary metabolites derived from the phenylpropanoid pathway. One type of flavonoid that is exclusively synthesized in the seed coat are proanthocyanidins or condensed tannins (Debeaujon *et al*., 2003). These colourless polyphenols coalesce into the central vacuole and, following cell death, they oxidize into brown complexes that cross-bond within the cell to produce the brown colour seen in mature *A. thaliana* seeds (Pourcel *et al*., 2005). Mucilage is another compound produced in large amounts by the *A. thaliana* seed coat. Mucilage is composed of pectin polysaccharides, primarily rhamnogalacturonan I (RGI), and its localized secretion to the plasma membrane forms a ring-shaped pocket under the outer epidermal cell wall (Haughn and Western, 2012). Upon imbibition of the dry, mature seed, this primary cell wall ruptures and the mucilage is extruded from its pocket. The mucilage forms an outer soluble layer and an inner adherent layer that contains cellulose microfibrils which interact with xylose side branches on RGI (Ralet *et al*., 2016). Similar to *A. thaliana*, the seed coat of mature *C. hirsuta* seeds is brown and extrudes mucilage upon imbibition; however, a detailed characterization of seed coat development has not yet been performed in this species.

Here, we characterize development of the *C. hirsuta* seed coat in relation to fruit and embryo development. In particular, we focus on the differentiation of distinctive features in the two outermost cell layers of the seed coat. We show that the epidermal oi2 layer accumulates mucilage, while the sub-epidermal oi1 layer determines the topography of the seed surface.

MATERIALS AND METHODS

Plant material and growth conditions

Cardamine hirsuta reference Oxford (OX) accession: herbarium specimen voucher Hay 1 (OXF) (Hay and Tsiantis, 2006). All plants were grown in long-day conditions in the greenhouse: 16 h light (22 °C), 8 h dark (20 °C). Whole fruits (stages 14, 15 and 16) and isolated seeds (stages 17a and 17b, and 1-year-old seeds dry or water imbibed) were processed in the laboratory for subsequent microscopy analyses.

Differential interference contrast (DIC) microscopy

Developing ovules and seeds were mounted in a chloral hydrate:glycerol:water (8:2:3) solution, allowed to clear overnight and viewed with a Zeiss Axio Imager Z1 (Carl Zeiss, Jena, Germany). Images were processed using ImageJ and Adobe Photoshop.

Clearing and staining of whole seeds with Nile red, Calcofluor white and basic fuchsin

For Nile red and Calcofluor white staining, seeds were first fixed in 4 % paraformaldehyde (PFA) in 0.05 M sodium cacodylate buffer (pH 6.9) at 4 °C overnight. After rinsing in the same buffer, seeds were cleared using 2,2'-thiodiethanol (TDE) (Musielak *et al*., 2016) or ClearSee, and simultaneously stained with either Nile red for suberin (Ursache *et al*., 2018) or Calcofluor white, a fluorescent probe for β-glycans (Mori and Bellani, 1996). To this end, seeds were incubated for 3 d in 0.05 % (w/v) Nile red (Santa Cruz Biotechnology, Dallas, TX, USA, sc-203747A) or 0.1 % (w/v) Calcofluor white (Fluorescent Brightener 28, Sigma-Aldrich Germany, F-3543), dissolved either in a solution of 65 % TDE, 25 % 0.2 M sodium cacodylate buffer and 10 % water or in ClearSee. Afterwards, seeds were rinsed thoroughly with and imaged in the respective clearing solution using a Zeiss LSM880 (Carl Zeiss, Jena, Germany). Basic fuchsin staining was performed according to method No. 1 described in Fuchs (1963) omitting steps 2 and 7. In brief, seeds were placed in 70 % ethanol at 60 °C for at least a day to extract chlorophyll. After rinsing in water, the seeds were cleared and stained for 12 h at 60 °C in a 1 % aqueous solution of basic fuchsin, to which 10 g of solid NaOH per 100 mL were added. After rinsing under slowly running tap water for at least 12 h, seeds were slowly dehydrated through a graded ethanol series (50, 70 and 95 %). The alcohol was then replaced with xylene or limonene and mounted in Entellan® (107960 Merck Millipore).

Scanning electron microscopy (SEM)

Samples were fixed overnight at 4 °C with 4 % (v/v) glutaraldehyde in 0.01 M phosphate buffer. After washing in buffer twice, samples were dehydrated through an ethanol gradient, critical-point dried using a Leica EM CPD300 and mounted onto stubs with double-sided adhesive tape. Mounted specimens were coated with gold using a Polaron SC 7640 sputter coater. For cryo-SEM, specimens were mounted onto copper holders with low temperature adhesive (Tissue-Tek, Sakura, 4583) and frozen in liquid nitrogen using a cryo-preparation device (K1250X, Emitech Technologies, Ringmer, UK). After sublimation of surface ice for 30 min, samples were sputter-coated with 80 % gold–20 % palladium (Polaron Sputter Coater SC 7600, Quorum Technologies). Samples were imaged with a Zeiss Supra 40VP SEM.

Chemical fixation and LR White resin embedding

For bright field and immunofluorescence microscopy, fruits and seeds were fixed with 2 % (v/v) paraformaldehyde and 2.5 % (v/v) glutaraldehyde in 0.1 M sodium cacodylate buffer (pH 6.9), supplemented with 0.025 % $CaCl_2$, for 3 h at room temperature, then kept overnight at 4 °C. After thorough rinsing in 0.1 M sodium cacodylate buffer (pH 6.9) and water, samples were dehydrated through an ethanol series and gradually embedded in medium-grade LR White resin (Plano GmbH, Wetzlar, Germany) over 5 d at room temperature. The resin was polymerized at 100 °C for 90 min (McDonald, 2014).

High-pressure freezing, freeze substitution and resin embedding

For transmission electron microscopy (TEM), fruits and seeds were processed by high-pressure freezing and freeze substitution (HPF-FS). Up to five seeds dissected from stage 17 fruit or ejected from exploding fruit, or 2 mm segments of stage 14, 15 and 16 fruit, were placed in aluminium specimen carriers with 300 µm deep cavities (Leica Microsystems GmbH), mounted in 1-hexadecene, capped with a second specimen carrier (flat side towards the sample) and immediately frozen using a Leica EM HPM 100 high-pressure freezer (Leica Microsystems GmbH). Seeds that had been dried for 1 year were imbibed in water overnight prior to freezing. Freeze-substitution in 2 % osmium tetroxide and 0.5 % uranyl acetate in acetone was performed in a Leica EM AFS2 freeze substitution device (Leica Microsystems GmbH) for ultrastructural observations (Micali *et al*., 2011). Once the samples reached room temperature, they were rinsed in acetone, carefully removed from the aluminium specimen carriers and gradually infiltrated in low viscosity epoxy resin (Science Services, Munich, Germany) or LR White resin (Plano GmbH, Wetzlar, Germany) for 6 d. Infiltration into pure resin was facilitated by ultracentrifugation (McDonald, 2014); resin polymerization was done in flat embedding moulds at 60 °C for 24 h.

Bright field microscopy of resin sections

For general tissue staining, semi-thin sections (1 µm) of fruits and seeds were collected on glass slides, stained with 1 % aqueous toluidine blue (O'Brien *et al*., 1964) supplemented with 1 % sodium tetraborate, and mounted permanently in Entellan® (107960 Merck Millipore). Staining of acidic lipids with 1 % (w/v) aqueous Nile blue A (Sigma-Aldrich Germany, N0766) was performed according to Spence (2001) with the following alterations: sections were dried down on diagnostic adhesion slides (Thermo Fisher Scientific X2XER202W# AD CE) and used without resin removal; staining was for 2 h; sections were mounted in anti-fade reagent Citifluor AF1 (Agar Scientific, UK). Images were taken with a Zeiss Axio Imager Z1 (Carl Zeiss, Jena, Germany).

Transmission electron microscopy

Ultrathin (70–90 nm) sections were collected on nickel slot grids as described (Moran and Rowley, 1988) and stained with 2 % (w/v) aqueous uranyl acetate for 10 min, followed by lead citrate for 15 min (Reynolds, 1963). Micrographs were taken with a Hitachi H-7650 transmission electron microscope (Hitachi High-Technologies Europe GmbH, Krefeld, Germany) operating at 100 kV fitted with an AMT XR41-M digital camera (Advanced Microscopy Techniques, Danvers, MA, USA).

Immunofluorescence and immunogold labelling

The following antibodies were used to detect different cell wall epitopes: CCRC-M36, recognizing epitopes residing on the unbranched RGI backbone (Pattathil *et al*., 2010); CCRC-M38, binding to fully de-esterified homogalacturonan (HG) epitopes with a degree of polymerization >5 (Pattathil *et al*., 2010); JIM7, labelling partially methyl esterified HG epitopes (Knox *et al*., 1990); and LM25, detecting (galactosylated) xyloglucans (Pedersen *et al*., 2012). For immunofluorescence labelling, semi-thin sections (1 µm) of chemically fixed, LR White-embedded samples were dried down on diagnostic adhesion slides (Thermo Fisher Scientific X2XER202W# AD CE) and incubated overnight at 4 °C in 5 % goat serum in Tris buffer (20 mM Tris, 225 mM NaCl, pH 6.9) supplemented with 1 % (w/v) bovine serum albumin (Tris-BSA). After three washes for 10 min in Tris-BSA, sections were incubated in a 1:20 dilution of CCRC-M36 or CCRC-M38, or in a 1:5 dilution of LM25, for 1 h at room temperature, and then washed again in Tris-BSA (3× 10 min). Subsequently, sections were incubated with appropriate secondary antibodies conjugated to Alexa Fluor 488® (goat anti-mouse IgG, 1:50, abcam ab150117; goat anti-rat IgG, 1:100, Life Technologies A-11006) for 1 h. Sections were washed in Tris-BSA (3× 10 min) and then mounted in anti-fade reagent Citifluor AF1 (Agar Scientific, UK). After mounting, slides were immediately imaged or stored at 4 °C in darkness and imaged the following day. For simultaneous double immunofluorescence labelling, primary antibody incubation was in a mixture of CCRC-M36 (diluted 1:100) and JIM7 (diluted 1:10) in Tris-BSA. For detection of CCRC-M36 and JIM7, two secondary antibodies (diluted 1:50 each) were used simultaneously: goat anti-mouse IgG conjugated to Alexa Fluor 647® (abcam, ab150119) and goat anti-rat IgG conjugated to Alexa Fluor 488® (Life Technologies, A-11006). Otherwise, the same protocol applied as for single immunofluorescence labelling. The presence of cellulose was assessed by the binding of CBM3a, a crystalline cellulose-binding module (Blake *et al*., 2006), to semi-thin sections (1 µm) of chemically fixed, LR White-embedded samples in a three-stage immunolabelling technique (McCartney *et al*., 2004). Sections were sequentially incubated for 1 h at room temperature with (1) CBM3a in 1 % Tris-BSA (10–20 µg mL^{-1}); (2) mouse monoclonal anti-His (Sigma-Aldrich Germany, H-1029; diluted 1:100); and (3) goat anti-mouse IgG conjugated to Alexa Fluor 488® (abcam, ab150117; diluted 1:100). Sections were rinsed with 1% Tris-BSA after each incubation step. Final mounting was as described above. As negative controls for immunocytochemical labelling, the primary antibodies or probes were replaced by Tris-BSA. Sections were subjected to pectinase digestion (1 U mL^{-1}; Sigma-Aldrich Germany) prior to immunolabelling of xyloglucans and cellulose as indicated (Wilson *et al*., 2015). Images were taken with a Zeiss Axio Imager Z1 (Carl Zeiss, Jena, Germany).

Immunogold labelling was performed on ultrathin sections of samples processed by HPF-FS and embedded into low-viscosity resin as described (Micali *et al*., 2011). Primary antibodies CCRC-M38 and JIM7 were used at half strength. Goat anti-mouse and goat anti-rat IgGs conjugated with 10 nm colloidal gold (British Biocell International) were used as secondary antibodies, diluted 1:20. Grids were stained and viewed in the transmission electron microscope as described above.

RESULTS

Seed coat surface structure

Arabidopsis thaliana seeds have a spherical, oblong shape (Fig. 1A), while seeds of *C. hirsuta* are flattened longitudinally to form a disc shape (Fig. 1C). In *A. thaliana*, the seed surface is structured by the outer seed coat layer oi2: the central columella forms a raised bump in the centre of penta- to heptagonal cells with prominent anticlinal cell walls (Fig. 1B). Seed imbibition in aqueous fixative solution triggers mucilage release from these oi2 cells in both *A. thaliana* and *C. hirsuta* (Supplementary Data Fig. S1); therefore, we used cryo-SEM to study the surface topography of mature seeds. In contrast to *A. thaliana*, the seed surface of *C. hirsuta* is structured predominantly by the sub-epidermal cell layer oi1 (Fig. 1D–F). Thickened anticlinal cell walls in the oi1 layer form prominent ridges, especially at the margin of the disc-shaped seed (Fig. 1D, E). The anticlinal cell walls and central columella of the oi2 layer are still visible in *C. hirsuta* (Fig. 1D), particularly on the flat sides of the seed (Fig. 1F). However, in contrast to *A. thaliana* seeds, the anticlinal cell walls of the underlying oi1 cell layer form the major topographical features of the seed surface in *C. hirsuta*.

Co-ordination of fruit and seed development

To investigate how the surface topography of *C. hirsuta* seeds is formed, we undertook a detailed analysis of the development of the two outermost seed coat layers, oi1 and oi2. We first describe how seed coat development is co-ordinated with development of the fruit and seeds (Fig. 2). Fruit development begins at stage 14 (Roeder and Yanofsky, 2006) after double fertilization occurs within the embryo sac inside the developing ovule (Fig. 2A–C). At stage 15, the gynoecium elongates and extends beyond the top of all other floral organs (Fig. 2E). The embryo sac starts to bend and the ovule begins to assume an amphitropous shape with the micropyle positioned near the insertion of the funiculus (Fig. 2F, G). At stage 16, sepals, petals and stamens wither and fall from the fruit which continues to elongate (Fig. 2I). The embryo sac becomes increasingly curved and the shape of the ovule is now reminiscent of a premature seed (Fig. 2J, K). Stage 17 is a long stage during which the fruit matures completely. It is divided into two sub-stages, 17a and 17b. In stage 17a, the fruit elongates towards its final length (Fig. 2M). Stage 17b starts when the fruit begins to increase in width (Fig. 2Q). Seed size increases and the seed and the embryo undergo important developmental changes to reach maturity (compare Fig. 2N with R, and O with S). Fruit pods are competent to explode from stage 17b. Dispersal of the mature seeds occurs by explosive pod shatter from this stage onwards.

Upon fertilization, the seed coat starts to differentiate from the ovule integuments and chalazal tissues (Fig. 2D). At stage 15, the outer integument consists of two cell layers (oi2 and

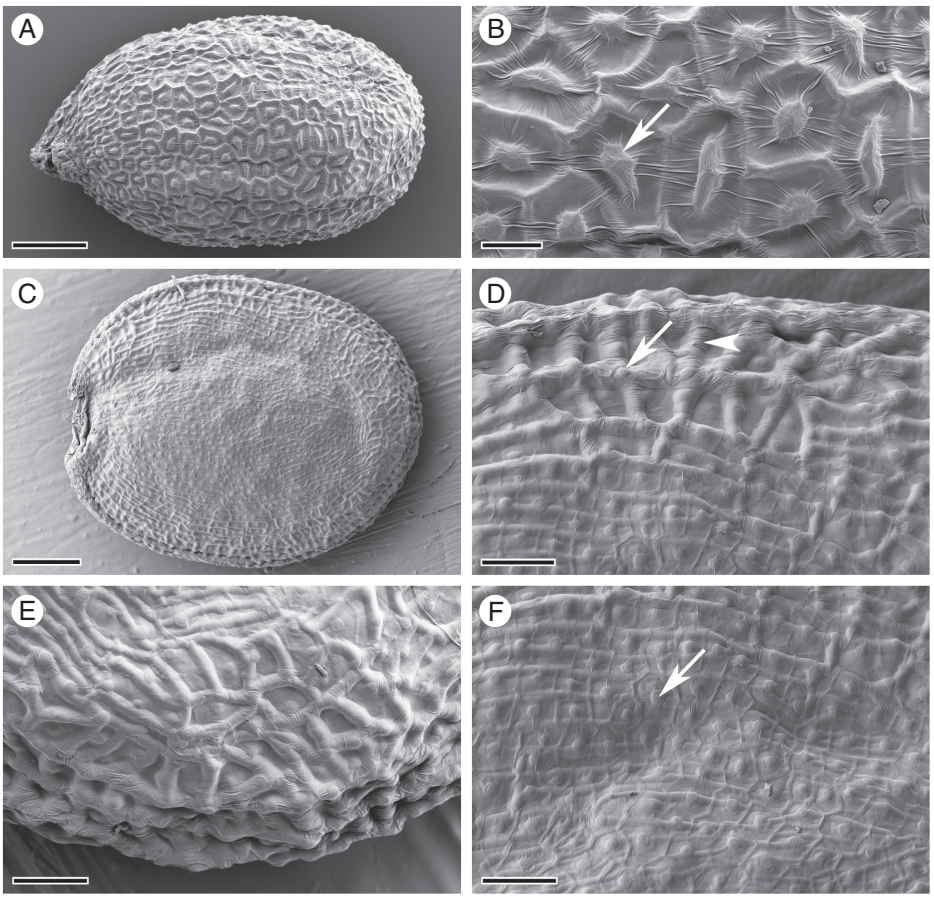

FIG. 1. Cryo-scanning electron micrographs of mature seed surface structure. (A, B) *A. thaliana* seed (A) and surface topography (B) consisting of columella (arrow) and anticlinal cell walls of epidermal oi2 cells. (C–F) *C. hirsuta* seed (C) and surface topography (D–F) characterized predominantly by anticlinal cell walls of the sub-epidermal seed coat layer oi1 (arrowhead, D), especially at the seed margin (E). The columella and anticlinal cell walls of oi2 cells are still visible (arrow, D, F), especially on the flat seed surfaces (F). Scale bars = 100 µm (A), 20 µm (B), 200 µm (C) and 50 µm (D–F).

oi1) and the inner integument of three cell layers (ii2, ii1' and ii1) (Fig. 2H). During subsequent development, all cell layers undergo dramatic changes and follow very different fates. The innermost layer (ii1), also called the endothelium, synthesizes large amounts of phenolic compounds which accumulate in the central vacuole (Fig. 2L, P, T) and are responsible for the brown colour of the mature seed coat (Supplementary Data Fig. S2). The other two layers of the inner integument (ii1' and ii2) do not differentiate further and are crushed during seed development (Fig. 2L, P, T). The two layers of the outer integument will give rise to the epidermal, mucilage-producing seed coat layer (oi2) and the sub-epidermal seed coat layer (oi1) characterized by prominent, asymmetric cell wall thickenings (Fig. 2T). It is the development and differentiation of these two outermost seed coat layers that we are most interested in and will describe further.

Co-ordination of seed coat and embryo development

At fruit stage 15, endosperm nuclei are dispersed throughout the embryo sac and appressed to the central cell wall by the large vacuole (Fig. 3A; free nuclear endosperm formation). Endosperm nuclei are regularly found within a pocket of cytoplasm at the chalazal pole (arrowhead, Fig. 3A). Embryos are globular and reach the 8-cell stage (Supplementary Data Fig. S3A). All five cell layers of the two ovule integuments are present at this stage (Fig. 3B). Cells of the ii1 layer are cytoplasmically dense and contain a large nucleus with a prominent nucleolus (arrowhead, Fig. 3B). Vacuoles of ii1 cells are still relatively small at this stage (Fig. 3B).

Apart from an increase in ovule size, the most obvious changes during fruit stage 16 are visible in the ii1 cell layer and the embryo (Fig. 3C, D). Embryos are still globular but cell number has increased noticeably (Fig. 3C; 32-cell stage). The vacuoles of ii1 cells have increased in size and started to accumulate phenolic compounds, visible in the turquoise colour of the vacuolar content after toluidine blue staining of semi-thin sections (arrowhead, Fig. 3D).

At fruit stage 17a, embryos transition through heart and torpedo stages (Fig. 3E). The embryo is about half as long as the seed length at the early torpedo stage (Fig. 2O) and continues to grow in length during stage 17a. Cellularization of the endosperm is first observed at fruit stage 17a when the embryo develops from heart shaped to torpedo shaped (Fig. 3E–G; Supplementary Data Fig. S3). Vacuoles of ii1 cells continue to fill with more phenolic compounds (arrowhead, Fig. 3F) and layers ii1' and ii2 of the ovule inner integument

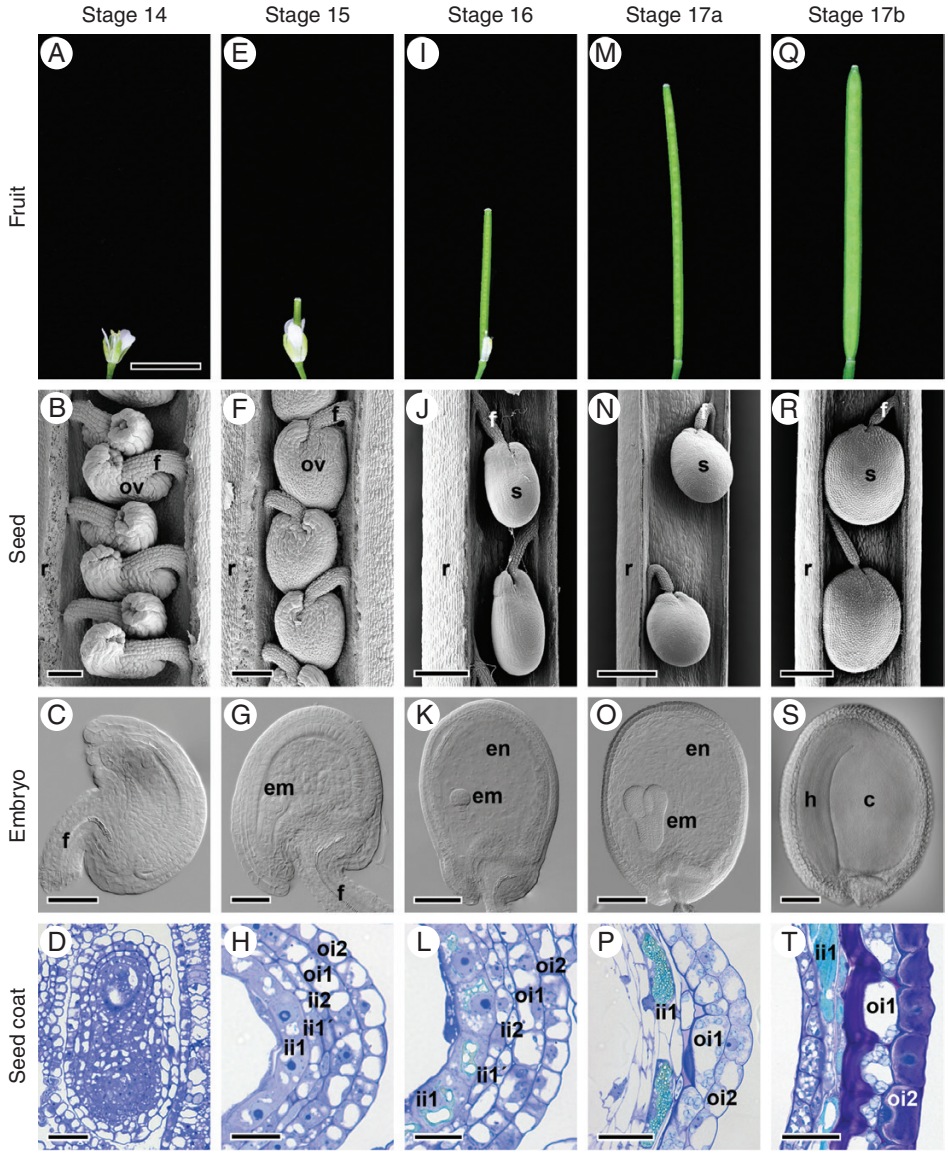

FIG. 2. Fruit and seed development in *C. hirsuta*. Stages of fruit development: 14 (A), 15 (E), 16 (I), 17a (M) and 17b (Q). Scanning electron micrographs of developing ovules and seeds in fruit at stages 14 (B), 15 (F), 16 (J), 17a (N) and 17b (R); covering valves were dissected off. DIC images of cleared ovules and seeds isolated from fruit at stages 14 (C), 15 (G), 16 (K), 17a (O) and 17b (S). Seed coat development shown in bright field images of toluidine blue-stained transverse LR White sections of chemically fixed fruits at stages 14 (D), 15 (H) and 16 (L), and seeds isolated from fruit at stages 17a (P) and 17b (T). Abbreviations: c, cotyledon; em, embryo; en, endosperm; f, funiculus; h, hypocotyl; ii, inner integument; oi, outer integument; ov, ovule; r, replum; s, seed. Scale bars = 5 mm (A, E, I, M, Q), 50 µm (B, C, D, G, P), 100 µm (F, K), 25 µm (H, L, T), 200 µm (J, O, S) and 400 µm (N, R).

are crushed (Fig. 3F, G). The seed starts to acquire a disc-shaped form (Fig. 2N) and, along the edge of the disc, the inner periclinal cell walls of oi1 cells begin to thicken slightly (arrowhead, Figs 3G and 4A). Cells of the seed coat epidermis, oi2, show no conspicuous signs of differentiation (Figs 3G and 4A, C).

Towards the end of fruit stage 17a, the embryo starts to bend (Fig. 3H). The seed coat is now composed of three layers (ii1, oi1 and oi2), and only towards the margin of the seed can remnants of layers ii1' and ii2 still be seen (arrow, Fig. 3I). Vacuoles of ii1 cells are almost completely filled with phenolic material (Fig. 3I). Cells of the two outermost layers oi2 and oi1 undergo dramatic changes. Asymmetric cell wall thickening in oi1 cells occurs exclusively on the inner periclinal cell wall and extends along the inner half of the anticlinal cell walls (Figs 3I and 4D). These cell wall thickenings are most conspicuous in cells at the margins of the disc-shaped seed (Figs 3H, I and 4D, G), in comparison with cells on the flat sides of the seed (Fig. 4E, F, H, I). It is also along the margins of the seed where the differentiation of epidermal oi2 cells is first observed (Figs 3I and 4D). The location of the nucleus changes from the bottom of oi2 cells to the centre of the outer periclinal wall (black arrowheads, Figs 3I and 4F). Mucilage secretion begins, forming a doughnut-shaped ring of mucilage (white arrowhead, Figs 3I and 4G–I) with the nucleus located in the 'hole of the doughnut'. At the periphery of the endosperm and

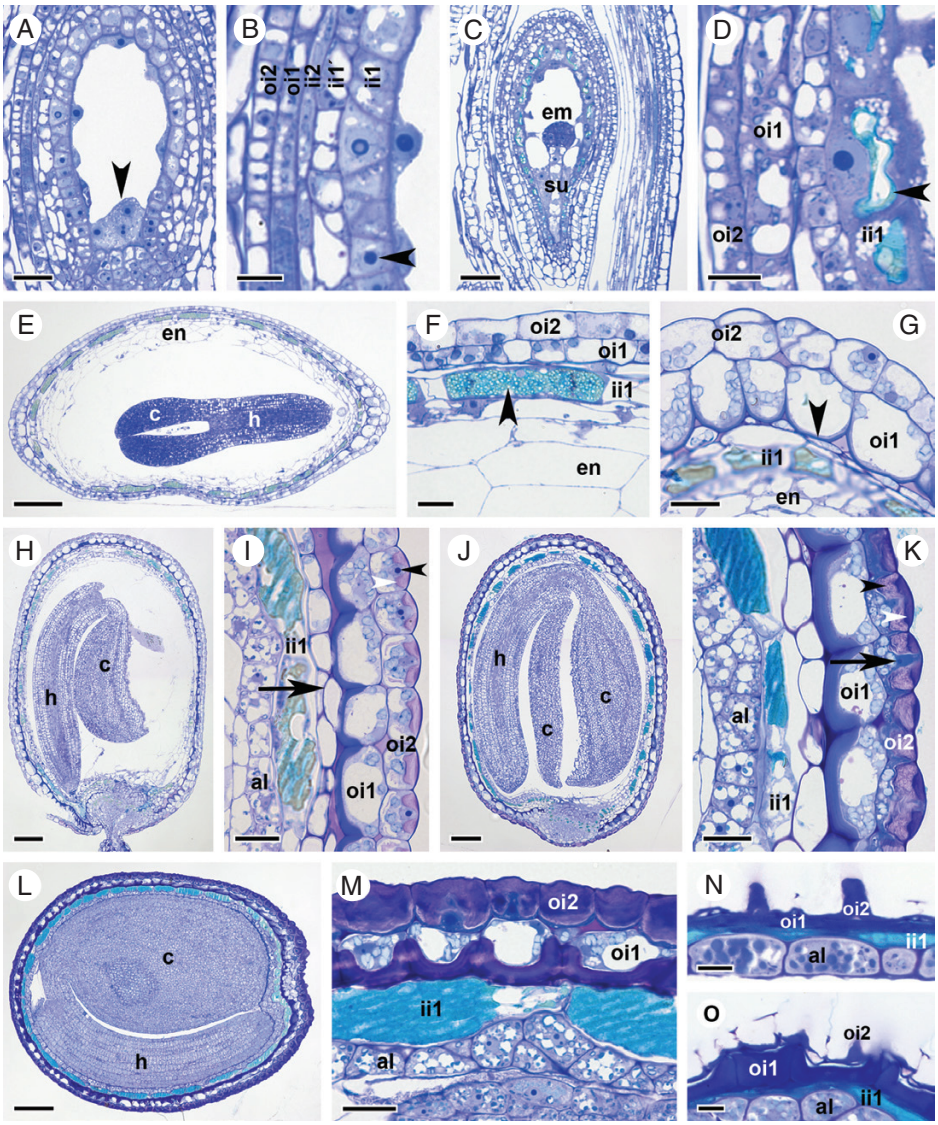

Fig. 3. Seed coat and embryo development in *C. hirsuta*. Bright field micrographs of toluidine blue-stained LR White sections of fruits and/or seeds after chemical fixation. (A, B) Stage 15 fruit. Fertilized ovule at the stage of free nuclear endosperm formation showing endosperm nuclei (arrowhead, A), a five-layered seed coat and a large nucleus with a prominent nucleolus in ii1 cells (arrowhead, B). (C and D) Stage 16 fruit. The globular embryo is attached to the suspensor (C). Vacuoles of ii1 cells start to accumulate phenolic compounds (arrowhead, D). (E–G) Seed from early stage 17a fruit with torpedo-stage embryo and endosperm starting to cellularize (E). Three-layered seed coat composed of undifferentiated oi2 and oi1 cells and ii1 cells filled with phenolic compounds (arrowhead, F). Inner periclinal cell walls of oi1 cells at the seed margin begin to thicken (arrowhead, G). (H and I) Seed from late stage 17a fruit with nearly mature embryo bent forwards such that the flat surface of the cotyledons lies parallel to the flat surface of the seed (H). External oi2 cells display polar mucilage accumulation (white arrowhead, I) with the nucleus located in the centre of the ring of mucilage (black arrowhead, I). The outermost endosperm cells differentiate into the aleurone-like layer (I). Remnants of ii1' and ii2 cell layers are found at the seed margin (arrow, I). (J and K) Seed from early stage 17b fruit containing a mature embryo (J) that is enclosed by the aleurone-like cell layer and an increasingly differentiated seed coat (K). Note the layered appearance of mucilage deposited in oi2 cells (black and white arrowheads, K). Arrow indicates cytoplasmic column. (L and M) Seed from mid stage 17b fruit containing a fully differentiated embryo (L). The three-layered seed coat is located external to the aleurone layer (M). Large vacuoles in ii1 cells are filled with phenolic compounds. In contrast to oi2 cells, the cellular content of oi1 cells is still recognizable. (N and O) Seeds from exploded (late) stage 17b fruit. Seeds are desiccated and cellular content of all three seed coat layers is unrecognizable. On the flat seed surface, columella structures of oi2 cells are prominent (N) and, at the seed margin, periclinal cell wall thickenings in oi1 cells are noticeable (O). Abbreviations: al, aleurone-like layer; c, cotyledon; em, embryo; en, endosperm; h, hypocotyl; ii, inner integument; oi, outer integument, su, suspensor. Scale bars = 20 µm (A, F, G, I, K, M), 10 µm (B, D, N, O), 50 µm (C) and 100 µm (E, H, J, L).

in contact with the ii1 layer, an aleurone-like cell layer begins to differentiate (Fig. 3I).

In the seeds of stage 17b fruit, the embryo continues to grow and the space between the two cotyledons and the hypocotyl becomes increasingly restricted (Fig. 3J). Cells of the aleurone-like layer are now easily distinguishable from the rest of the endosperm (Fig. 3K). Secretion of mucilage in oi2 cells and asymmetric cell wall thickening of oi1 cells continues (Figs 3K and 4J–L). In semi-thin sections of chemically fixed samples stained with toluidine blue, the mucilage in oi2 cells is not uniformly stained – an outer, dense portion stains dark purple (white arrowhead, Fig. 3K) and an inner,

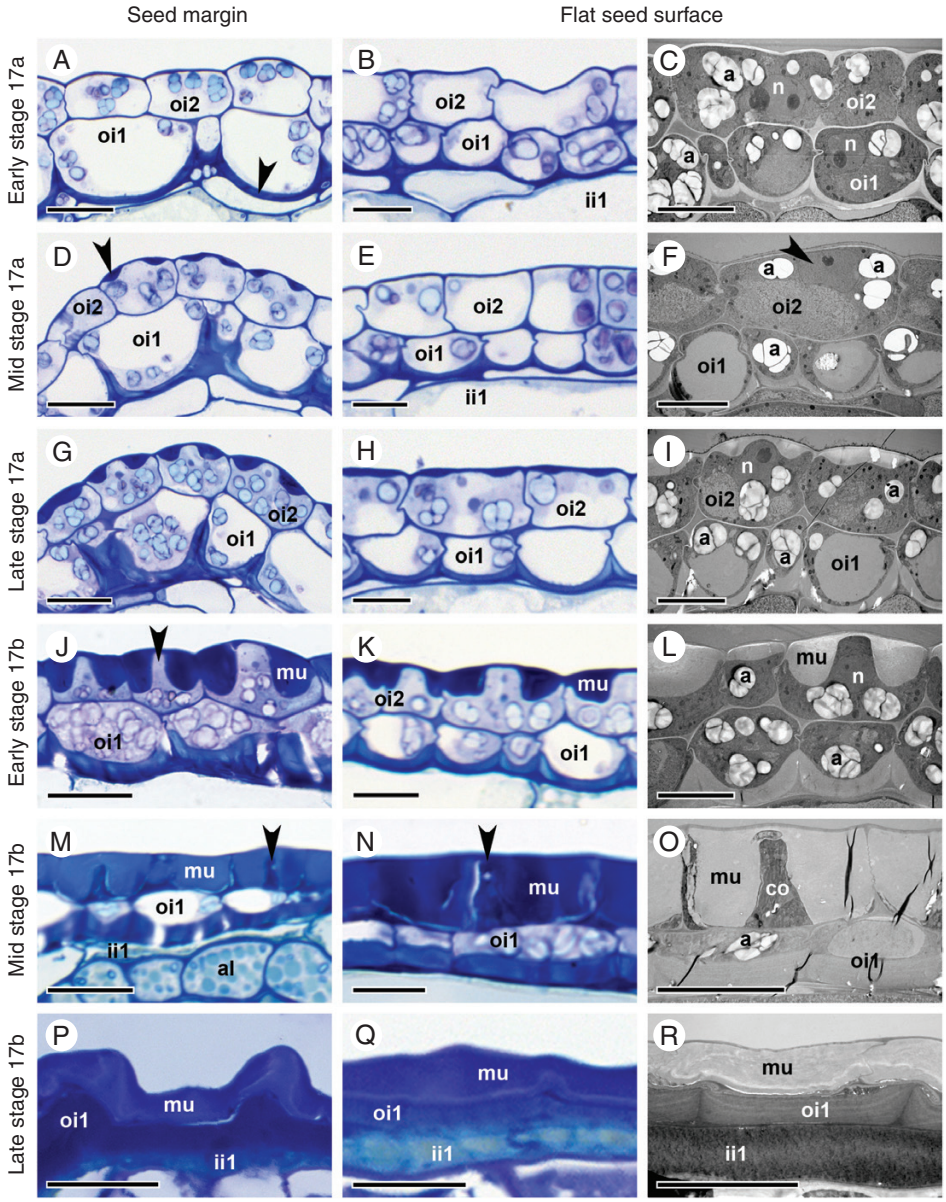

FIG. 4. Differentiation of the two outermost seed coat layers, oi2 and oi1, during stage 17 of *C. hirsuta* fruit development. Bright field and transmission electron micrographs of HPF-FS-processed samples showing cells at the seed margin (left column) and at the flat seed surfaces (middle and right columns). (A–C) Early stage 17a. Undifferentiated oi2 cells. Polar deposition of cell wall material occurs on the inner periclinal wall of oi1 cells, especially at the seed margin (arrowhead, A). Amyloplasts are present in oi1 and oi2 (C). (D–F) Mid stage 17a. Mucilage secretion is first visible in oi2 cells at the seed margin (arrowhead, D) and is preceded by the migration of the nucleus towards the centre of the outer periclinal cell wall (arrowhead, F). The inner periclinal wall of oi1 cells continues to thicken. In oi1 cells at the seed margin, thickening extends halfway up the anticlinal walls (D). Amyloplasts are present in oi1 and oi2 (F). (G–I) Late stage 17a. Mucilage secretion is visible in all oi2 cells. Asymmetric cell wall thickening continues in oi1 cells. Amyloplasts are present in oi1 and oi2 (I). (J–L) Early stage 17b. Mucilage accumulation in oi2 cells extends towards the inner periclinal cell wall, constricting the cytoplasm into a columnar shape (columella, arrowhead, J). Asymmetric cell wall thickening continues in oi1 cells. Amyloplasts are present in oi1 and oi2 (L). (M–O) Mid stage 17b. Mucilage extends from the outer to the inner periclinal cell wall in oi2 cells, surrounding the columella (arrowheads). No organelles are present in oi2 cells. Amyloplasts are still present in oi1 cells (O). The inner periclinal cell wall in oi1 cells is now very thick. (P–R) Late (exploded) stage 17b. The seed coat is desiccated. The oi2 layer mainly consists of mucilage, the oi1 layer of periclinal and anticlinal cell wall thickenings and the ii1 layer of phenolic compounds. Abbreviations: a, amyloplast; al, aleurone-like layer; co, columella; ii, inner integument; mu, mucilage; n, nucleus; oi, outer integument. Scale bars = 20 µm (A, D, G, J, M, P) and 10 µm (B, C, E, F, H, I, K, L, N, O, Q, R).

more loosely structured portion, stains a light purple colour (black arrowhead, Fig. 3K). Due to the large amount of mucilage, the cellular content of oi2 cells is severely restricted and forced into a columnar shape in the cell centre (arrow, Fig. 3K and arrowhead Fig. 4J). This cytoplasmic column (columella) extends from the outer to the inner periclinal walls and into the space adjacent to the inner periclinal cell wall. The cytoplasmic space is largely filled by the nucleus in the columella and numerous amyloplasts between the mucilage and the inner periclinal cell wall (Figs 3K and 4J–L). In contrast, oi1 cells are less constricted and the central vacuole is still discernible (Figs 3K and 4J–L).

In seeds during later stages of 17b fruit, the embryo reaches its final size, with little space left between the cotyledons and the hypocotyl (Fig. 3L). The endosperm is consumed almost completely, leaving only the peripheral aleurone-like cell layer between the embryo and the ii1 cell layer of the seed coat (Fig. 3M; aleurone-like cells contain numerous protein storage vacuoles and amyloplasts enclosing starch grains). Cells in the ii1 layer are now completely filled with phenolic compounds (Fig. 3M). Mucilage fills almost the entire volume of oi2 cells, with the exception of the central columella (Figs 3M and 4M–O). Organelles are no longer distinguishable in oi2 cells, and a completely crushed layer of cytoplasm is pushed against the inner periclinal cell wall (Figs 3M and 4M–O). The asymmetric cell wall in oi1 cells has thickened further (Fig. 4M–O) and stains a much darker colour in semi-thin sections of chemically fixed material after toluidine blue staining (Fig. 3M). In contrast to oi2 cells, oi1 cells are still alive at this stage with discernible vacuoles and numerous amyloplasts filling the cytoplasmic space (Figs 3M and 4O).

At the point when stage 17b fruit explode, the seed coat of ejected seeds is identical to that of completely dried seeds, with all cells in the remaining ii1, oi1 and oi2 layers dead (Figs 3N, O and 4P–R). Phenolic compounds are released from ii1 cells (turquoise colour in toluidine blue-stained semi-thin sections, Fig. 3N, O). In *A. thaliana*, these compounds are flavonoids called proanthocyanidins (Lepiniec *et al*., 2006). Their oxidation during seed desiccation leads to the formation of brown pigments that colour the mature seeds and promote longevity and dormancy (North *et al*., 2010). Preparation of *C. hirsuta* seeds at this stage of development is difficult due to these chemical barriers in the seed coat that prevent diffusion of fixatives and subsequent resin impregnation. The cell walls of oi1 and oi2 cells are all that remain of the desiccated seed coat, with the columella of oi2 cells prominent on the flat seed surfaces (Fig. 3N), and the asymmetric cell wall thickenings of oi1 cells particularly prominent at the seed margins (Fig. 3O).

To study subcellular events during seed coat development and to preserve cellular structures close to their native state and with minimum artefacts, we processed seeds from stage 17 fruit, including exploded fruit, by means of HPF-FS (Figs 4 and 6–10). High-pressure freezing cryo-immobilizes all molecules and avoids damage caused by conventional chemical fixation. When comparing toluidine blue-stained semi-thin sections of samples processed by chemical fixation (Fig. 3) and HPF-FS (Fig. 4), two differences are striking. In HPF-FS samples, mucilage secreted in oi2 cells stains homogenously with toluidine blue, and the vacuolar content of ii1 cells does not stain turquoise with toluidine blue. These observations can be explained by the nature of fixatives used for each method. While seeds are submerged in an aqueous medium for chemical fixation, they are substituted in a polar solvent during FS after HPS. As a consequence, mucilage in oi2 cells starts taking up water from the aqueous fixative solution during chemical fixation (Fig. 3; Supplementary Data Fig. S1) while remaining structurally unaltered in the organic solvent of the FS cocktail (Fig. 4). On the other hand, phenolic compounds present in the vacuoles of ii1 cells have only a limited solubility in water but are soluble in most organic solvents. Therefore, phenolic compounds are still present in ii1 cell vacuoles after chemical fixation and stain prominently in toluidine blue-stained semithin sections (Fig. 3). In contrast, phenolic compounds have been dissolved by the organic solvent during freeze substitution and show little colour in toluidine blue-stained semi-thin sections (Fig. 4).

Immunocytochemical analysis of oi2 and oi1 cell walls

Differentiation of the outermost seed coat layers, oi2 and oi1, in *C. hirsuta* involves polar deposition of pectic compounds (Figs 3 and 4). Both the mucilage in oi2 cells and the cell wall thickenings in oi1 cells stain similarly with toluidine blue in semi-thin sections (Figs 3 and 4). Therefore, to further characterize and distinguish the pectin composition of these two seed coat layers, we probed semi-thin sections of chemically fixed seeds at stage 17b with various antibodies that recognize the pectic cell wall component HG [JIM7 (Knox *et al*., 1990) and CCRC-M38 (Pattathil *et al*., 2010)] and RGI, the pectic component of seed coat mucilage (CCRC-M36; Young *et al*., 2008). We first performed single immunofluorescence labelling of consecutive sections (Fig. 5A–D). CCRC-M36 exclusively labels the mucilage in oi2 cells (Fig. 5A, B), while in an adjacent section, CCRC-M38 reacts very strongly with the asymmetrically thickened cell wall of oi1 cells but does not label the mucilage in oi2 cells (Fig. 5C, D). CCRC-M38 shows a homogenous signal throughout the thickened periclinal cell wall of oi1 cells and labels all cell walls of the seed including the embryo (Fig. 5D). To confirm that distinct pectic components can be recognized in the walls of oi2 vs. oi1 cells, we performed simultaneous double immunofluorescence labelling (Fig. 5E–G). For this, we used CCRC-M36, a mouse monoclonal antibody, in combination with JIM7, a rat monoclonal antibody. We verified that CCRC-M36 exclusively labelled mucilage pockets in oi2 (red, Fig. 5E–G), while JIM7, similar to CCRC-M38, reacted strongly with the asymmetrically thickened cell wall of oi1 cells and labelled all cell walls of the seed coat (green, Fig. 5E–G). CCRC-M36 signal only labels the outer, denser part of the mucilage (red, Fig. 5F, G) that stains dark purple with toluidine blue on semi-thin sections of chemically fixed seeds (Fig. 3K).

To further distinguish the specialized cell walls of oi2 and oi1 cells, we used probes to detect cellulose (His-tagged crystalline cellulose-binding module, CBM3a; Blake *et al*., 2006) and the hemicellulose xyloglucan (LM25; Pedersen *et al*., 2012). Thickened oi1 cell walls contained both cellulose and xyloglucan (arrows, Fig. 5H, I), whereas the mucilage pockets in oi2 cells were devoid of CBM3a and LM25 labelling (arrowheads, Fig. 5H). Fluorescence signal intensities of both probes were significantly increased by epitope unmasking after pectinase treatment (see insets imaged with identical settings to main panel, Fig. 5H, I).

Mucilage accumulation in oi2 cells of the C. hirsuta seed coat

Cells of the outer seed coat layer, oi2, develop from relatively non-distinct parenchymatous cells into highly specialized cells that accumulate large amounts of mucilage in a specific cell wall domain (Fig. 6A–C). Mucilage is secreted into a doughnut-shaped pocket between the outer periclinal cell wall

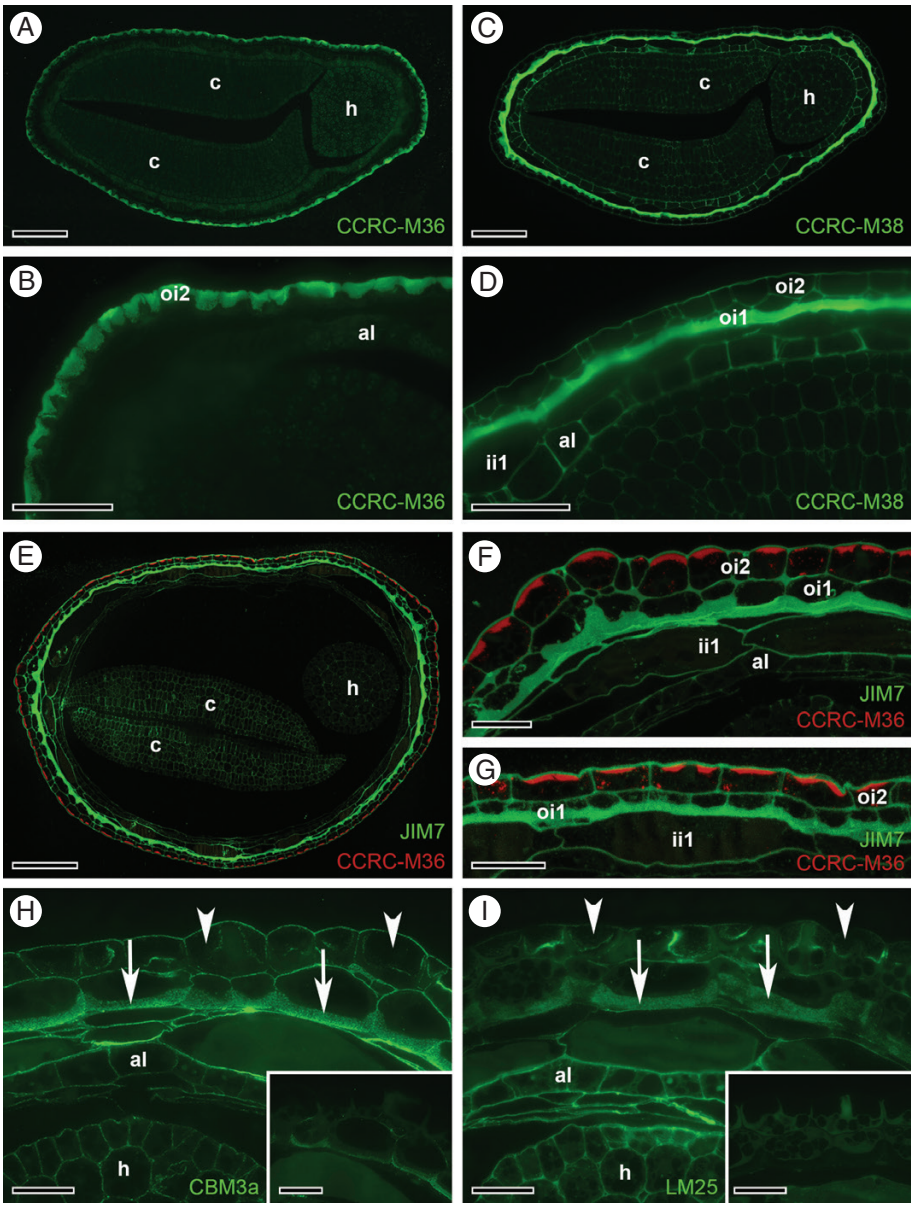

Fig. 5. Immunofluorescence detection of pectin, cellulose and xyloglucan epitopes in oi2 and oi1 seed coat cells at stage 17b of *C. hirsuta* fruit development. (A–D) Consecutive transverse LR White sections. (A and B) CCRC-M36 reacts against the unbranched backbone of rhamnogalacturonan I (RGI) pectins, and binds exclusively to mucilage in oi2 cells. (C and D) CCRC-M38 reacts with de-esterified homogalacturonan (HG) pectins, and binds to all cell walls of the seed but particularly strongly to the thickened inner periclinal cell walls of oi1 cells. (E–G) Simultaneous immunofluorescence detection of CCRC-M36 epitopes (red) in the mucilage of oi2 cells, and JIM7 epitopes (green, JIM7 reacts with methyl esterified HG pectins) in the thickened inner periclinal cell walls of oi1 cells. (H and I) After pectin unmasking, the cellulose-binding probe CBM3a (H), and LM25 (I), which recognizes xyloglucans, react with thickened oi1 cell walls (arrows) and all other cell walls of the seed, but do not react with mucilage in oi2 cells (arrowheads). Without pectin unmasking, the signal is weak or absent under identical imaging parameters (insets, H and I). Abbreviations: al, aleurone-like layer; c, cotyledon; h, hypocotyl; ii, inner integument; oi, outer integument. Scale bars = 100 µm (A, C, E), 50 µm (B, D) and 25 µm (F, G), 20 µm (H, I, including insets).

and the plasma membrane (Fig. 6B). This ring of mucilage extends down into the cell and appears as two large pockets of mucilage in cross-section (Fig. 6C). The nucleus is initially located at the inner periclinal cell face (Fig. 6A) but relocates to the centre of the doughnut-shaped pocket of mucilage in close proximity to the outer cell wall (Fig. 6B, C). Oi2 cells possess amyloplasts with large starch granules (Fig. 6A, B) that cluster at the inner periclinal cell face as the mucilage pocket enlarges (Fig. 6C). The lytic vacuole decreases in size at the onset of oi2 cell differentiation, and material of fibrillar appearance becomes visible in the remaining vacuolar lumen (Fig. 6B).

Primary cell walls of oi2 cells are strongly labelled by antibodies that recognize methyl esterified pectin (JIM7, Fig. 6D, E) and de-esterified pectin (CCRC-M38, Fig. 6F, G). While in undifferentiated oi2 cells, distribution of JIM7 epitopes is uniform throughout the thickness of the primary cell wall, CCRC-M38 labelling density decreases towards the plasma membrane (Fig. 6D, F). At later stages, when oi2 cells started to

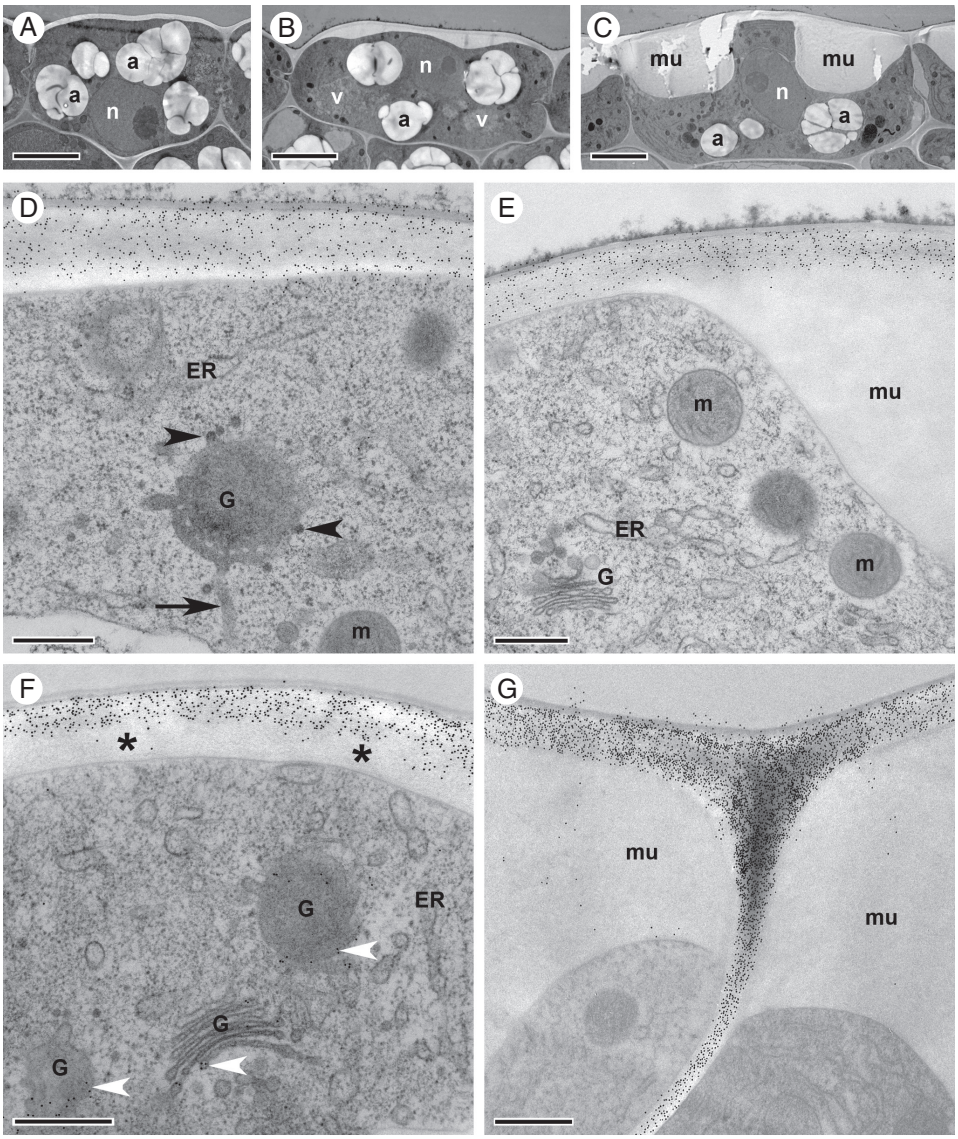

FIG. 6. Mucilage accumulation in oi2 seed coat cells during stage 17 of *C. hirsuta* fruit development. Transmission electron micrographs of transverse sections of HPF-FS-processed seeds showing cellular details and distribution of pectin epitopes in oi2 cells. (A–C) Overview of oi2 cell differentiation during early (A) and late stage 17a (B), and early stage 17b (C). (D–G) Indirect immunogold labelling of JIM7 epitopes (D and E) and CCRC-M38 epitopes (F and G). Both epitopes are abundant in the primary cell wall of undifferentiated (D and F, early stage 17a) and differentiated (E and G, early stage 17b) oi2 cells but absent from the mucilage (E and G). In undifferentiated oi2 cells, CCRC-M38 epitopes are absent from younger parts of the cell wall (asterisk in F) but present in the Golgi (white arrowheads in F). Note tubules connected to the rim of the Golgi cisternum (arrow, D) as well as dense vesicles budding off (arrowheads, D). Abbreviations: a, amyloplast; ER, endoplasmic reticulum; G, Golgi stack; m, mitochondrion; mu, mucilage; n, nucleus; v, vacuole. Scale bars = 5 µm (A–C) and 500 nm (D–G).

differentiate, primary cell walls label uniformly for both methyl esterified and de-esterified pectins (Fig. 6E, G). In contrast, the mucilage deposited between the primary cell wall and the plasma membrane is not labelled above background by either JIM7 or CCRC-M38 antibodies (Fig. 6E, G). Pectins are synthesized and modified by Golgi-localized enzymes and we could detect CCRC-M38 epitopes in Golgi stacks (white arrowheads, Fig. 6F). While the CCRC-M36 antibody reacted strongly and specifically with oi2 cell mucilage in chemically fixed seeds (Fig. 5A, B, E–G), immunogold labelling was only slightly above background in HPF-FS-processed seeds (Supplementary Data Fig. S4). It is likely that CCRC-M36 binding was inhibited by our osmium fixation, as immunolabelling of non-osmicated *A. thaliana* seeds with CCRC-M36 has been shown previously (Young *et al.*, 2008).

Mucilage secretion is accompanied by increased Golgi activity and microtubule rearrangement

The most prominent ultrastructural feature of oi2 cells during mucilage secretion is the large number of highly differentiated Golgi stacks (Fig. 7A). The organization of the Golgi is complex, especially at the *trans* side which is composed of a network of

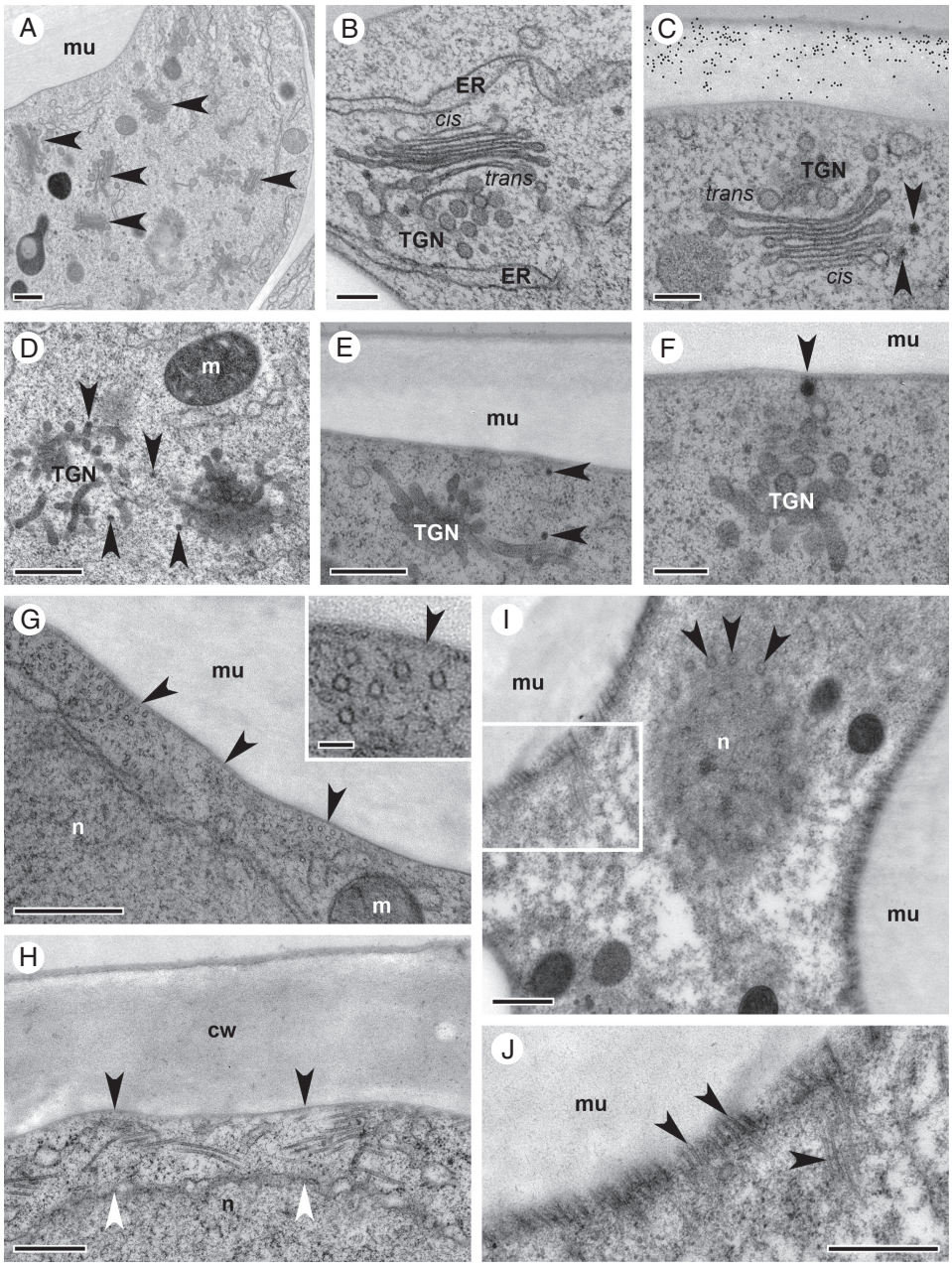

FIG. 7. Ultrastructural rearrangements during mucilage secretion in oi2 seed coat cells during stage 17 of *C. hirsuta* fruit development. Transmission electron micrographs of transverse sections of HPF-FS-processed seeds showing ultrastructural details of Golgi stacks and cortical microtubules. (A) Overview showing the abundance of Golgi stacks (black arrowheads) in oi2 cells during mucilage secretion. (B and C) Cross-sections through Golgi stacks with clear polarity between the *cis* and *trans* sides marked by a prominent *trans*-Golgi network (TGN). Black arrowheads indicate dense vesicles at the *cis* side of the Golgi that are likely to be COPI vesicles; immunogold labelling of CCRC-M38 epitopes marks the cell wall (C). (D–F) Different views of the *trans* side of Golgi stacks characterized by prominent TGNs. Small, electron-dense vesicles (arrowheads) bud off from these tubules and can be seen in the cytoplasm (D and E) and adjacent to the outer plasma membrane (E and F). (G) Numerous microtubules (most of them cut in cross section – see also inset in G) are located underneath the plasma membrane (arrowheads) adjacent to the secreted mucilage in oi2 cells. (H) A dense network of microtubules spans between the plasma membrane (black arrowheads) and the nuclear envelope (white arrowheads) at the top of the cytoplasmic columella. (I and J) Tangential section through the cytoplasmic columella and the nucleus showing nuclear pores (arrowheads, I) and the dense array of microtubules adjacent to the mucilage (boxed region, I; arrowheads, J at increased magnification). Abbreviations: *cis*, *cis* side of the Golgi stack; ER, endoplasmic reticulum; cw, cell wall; TGN, *trans*-Golgi network; *trans*, *trans* side of the Golgi stack; m, mitochondrion; mu, mucilage; n, nucleus. Scale bars = 500 nm (A, D, E, G–J), 50 nm (inset in G) and 200 nm (B, C, F).

intricately connected tubules and vesicles (80 nm diameter), the so-called *trans*-Golgi network (TGN; Fig. 7B–F). The increase in the number of Golgi stacks and in the complexity of Golgi stack organization marks the onset of mucilage production in oi2 cells during stage 17a of fruit development. Golgi stacks persist through to stage 17b, at which point the density of Golgi stacks in the cytoplasm increases further due to constriction of the protoplast caused by ongoing mucilage production (Fig. 7A).

A Golgi stack is usually composed of about five to six cisternae in oi2 cells during mucilage secretion (Fig. 7B). The

central part of the cisternae becomes narrower from the *cis* to the *trans* side of the stack and the margins of all cisterna are swollen (Fig. 7B). Vesicles budding off from or fusing with individual cisternae can be seen throughout the stack (Fig. 7B). Dense vesicles (40 nm diameter) can be seen in the vicinity of Golgi stacks that may correspond to coat protein complex I (COPI) vesicles (Donohoe *et al*., 2007) (Fig. 7C), but also scattered throughout the cytoplasm and close to the plasma membrane (Fig. 7D–F). Different planes of section through Golgi stacks offer very different views: (1) a stack of cisternae in cross-section (Fig. 7B); (2) large, round cisternae with dense vesicles budding off from the fenestrated rim in sections running parallel through more *trans*-located cisternae (Fig. 6D); and (3) clusters of interconnected vesicles and tubules in sections only hitting the *trans* side of the Golgi stack (Fig. 7D–F).

Another prominent ultrastructural feature is the abundance of microtubules directly beneath the plasma membrane lining the mucilage secretion domain (Fig. 7G). A very large number of microtubules are present in the limited space between the nucleus and the plasma membrane at the top of the cytoplasmic column (Fig. 7H) and can be easily seen in tangential sections of the columella in the vicinity of the nucleus (Fig. 7I, J).

The cytoplasm of oi2 cells also contains several amyloplasts with prominent starch granules (Fig. 6A–C), numerous mitochondria and strands of rough enoplasmic reticulum (ER; Fig. 6D, E). The ER is shaped like a string of pearls in longitudinal section (Fig. 6E; Supplementary Data Fig. S5A), although the ER often appears more dilated in high-pressure-frozen samples than in chemically fixed samples (Robinson *et al*., 2015; Pain *et al*., 2019). In the central columella, abundant ER sheets are seen between the nucleus and the plasma membrane delimiting the top of the columella (Supplementary Data Fig. S5B). In addition to dense vesicles and vesicles that are part of the *trans* side of the Golgi (Fig. 7C–F), clathrin-coated vesicles can be detected more frequently in the cytoplasm of oi2 cells during late stage 17a and early stage 17b of fruit development (Supplementary Data Fig. S5C). The exact function of these clathrin-coated vesicles in the vicinity of the TGN is unclear, but may indicate transport to the lytic vacuole and/or recycling of plasma membrane-resident proteins back to the cell surface (Robinson and Pimpl, 2014). At this stage of development, multivesicular bodies also become more numerous (Supplementary Data Fig. S5D) and large amounts of lipid storage vacuoles start to accumulate (Supplementary Data Fig. S6). These are first seen as spherical vacuoles scattered throughout the cytoplasm (Supplementary Data Fig. S6A) and sometimes connected to the ER (arrowheads, Supplementary Data Fig. S6B). As oi2 cell differentiation progresses, they appear to form larger compartments of very irregular shape (Supplementary Data Fig. S6B–F).

Asymmetric cell wall thickenings in oi1 cells of the C. hirsuta seed coat

Cells of the inner seed coat layer develop from relatively non-distinct parenchymatous cells to highly specialized cells that deposit a thick cell wall asymmetrically in the cell (arrowheads, Fig. 8A–C). This thickened cell wall is deposited along the inner periclinal cell wall and extends part way along the anticlinal cell walls of oi1 cells. The extent of thickening along the anticlinal cell walls depends on whether cells are located around the margin or on the flat sides of the disc-shaped seed. On the seed's flat sides, cell wall thickenings are restricted mainly to the inner periclinal cell wall (Fig. 8B, C). In contrast, around the margin, cell wall thickenings extend along the anticlinal cell walls, forming a U-shape in cross-section (Fig. 3M). In addition to the extent along the anticlinal cell wall, the total cell wall thickness also depends on the exact location of oi1 cells in the seed (Figs 3 and 4).

As in primary cell walls of differentiated and undifferentiated oi2 cell walls (Fig. 6), immunogold labelling of thickened oi1 cell walls with the anti-pectin antibodies JIM7 and CCRC-M38 showed that the two antibodies reacted slightly differently with the pectins in this thick, inner periclinal cell wall. JIM7 epitopes were evenly distributed over the total thickness of the oi1 cell walls, including middle lamellae and primary cell walls, at stages 17a and early 17b of *C. hirsuta* fruit development (Fig. 8D, E). In contrast, CCRC-M38 was restricted to middle lamellae and primary cell walls at stage 17a (Fig. 8F). Prominent oi1 cell wall thickenings show stronger CCRC-M38 labelling during early stage 17b in a gradient that decreases from the middle lamellae towards the younger parts of the cell wall adjacent to the plasma membrane (Fig. 8G). This may reflect a differential pattern in the degree of methyl esterification of the pectins constituting the thickened cell wall recognized by the two antibodies (Knox *et al*., 1990; Pattathil *et al*., 2010). However, since we observed no difference between the labelling pattern of JIM7 and CCRC-M38 in chemically fixed seeds (Fig. 5), this result may reflect partial inhibition of CCRC-M38 binding by our osmium fixation.

Golgi stacks produce pectins that are deposited in thickened oi1 cell walls

Similar to the differentiation of oi2 cells, an increase in the number of Golgi stacks clearly marks the onset of cell wall thickening in oi1 cells (Fig. 9A). Numerous Golgi stacks are present in oi1 cells throughout stage 17 of fruit development, in addition to multivesicular bodies and an extended ER network with slightly dilated tubules due to HPF-FS processing (Fig. 9A).

Having shown that anti-pectin antibodies label the thickened periclinal cell wall in oi1 cells (Figs 5 and 8), we used the same antibodies to follow the production of these pectin epitopes in Golgi stacks within the cell. Golgi stacks were immunogold labelled by both JIM7 and CCRC-M38 during oi1 cell differentiation (Fig. 9B–D). Both epitopes were most abundant in the swollen margins of mid- and *trans*-located cisternae (arrowheads, Fig. 9B–E). We could detect JIM7 epitopes in vesicles that can be seen fusing with or in close contact with the plasma membrane adjacent to newly deposited cell wall thickenings (arrow, Fig. 9E).

In contrast to the abundance of microtubules lining the plasma membrane during mucilage secretion in oi2 cells (Fig. 7G–J), few microtubules were detected in the vicinity of the plasma membrane adjacent to cell wall thickenings in oi1 cells (Fig. 9F).

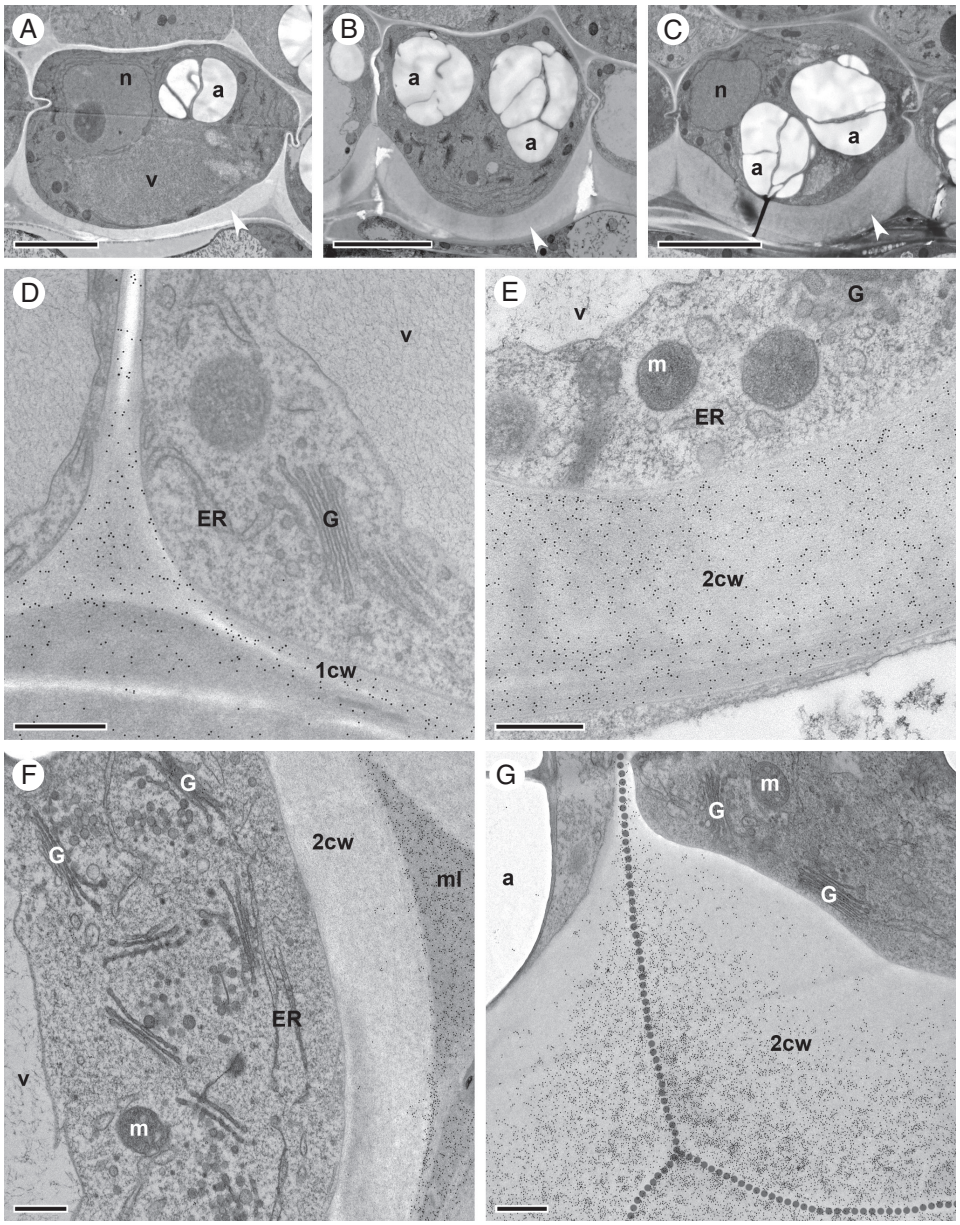

FIG. 8. Asymmetric cell wall thickening in oi1 seed coat cells during stage 17 of *C. hirsuta* fruit development. Transmission electron micrographs of transverse sections of HPF-FS-processed seeds showing cellular details and distribution of pectin epitopes in oi1 cells. (A–C) Overview of oi1 cell differentiation during early (A) and late stage 17a (B), and early stage 17b (C). Thickened inner periclinal cell wall is indicated by white arrowheads. (D–G) Indirect immunogold labelling of JIM7 epitopes (D and E) and CCRC-M38 epitopes (F and G). JIM7 epitopes are abundant and evenly distributed in the primary cell wall of undifferentiated oi1 cells (D, early stage 17a) as well as in the thickened inner periclinal cell wall of more differentiated oi1 cells (E, early stage 17b). CCRC-M38 epitopes are restricted to the middle lamellae of oi1 cells and absent from inner periclinal cell wall thickenings at early stages of differentiation (F, mid stage 17a). The density of CCRC-M38 epitopes in cell wall thickenings is graded towards the middle lamella (dotted line) in more differentiated oi1 cells (G, early stage 17b). Note the abundance of Golgi stacks in oi1 cells (B and F). Abbreviations: 1cw, primary cell wall; 2cw, thickened cell wall; a, amyloplast; ER, endoplasmic reticulum; G, Golgi stack; m, mitochondrion; ml, middle lamella; n, nucleus; v, vacuole. Scale bars = 5 µm (A–C) and 500 nm (D–G).

Thickened cell walls and mucilage comprise the mature seed coat

Cardamine hirsuta fruit are competent to eject their seeds by explosive pod shatter towards the end of stage 17b (Fig. 2). The seed coat of freshly ejected seeds is identical to that of completely dried seeds (Fig. 10), indicating that the seed coat is desiccated and development is complete at this stage. All cells in ii1, oi1 and oi2 layers are dead and the crushed cytoplasmic content of oi2 cells is visible (asterisk, Fig. 10A). The major difference between the seed coat of freshly ejected seeds and those removed from mid stage 17b fruit is the presence of a prominent secondary cell wall in the centre of oi2 cells (Fig. 10A). The formerly cytoplasmic columella is now completely occupied by cell wall material deposited between the mucilage and the plasma membrane (Fig. 10A). This is clearly illustrated by immunogold labelling with CCRC-M38 antibodies that label the primary and secondary cell walls of oi2 cells but not the mucilage secreted between these walls (Fig. 10A–C).

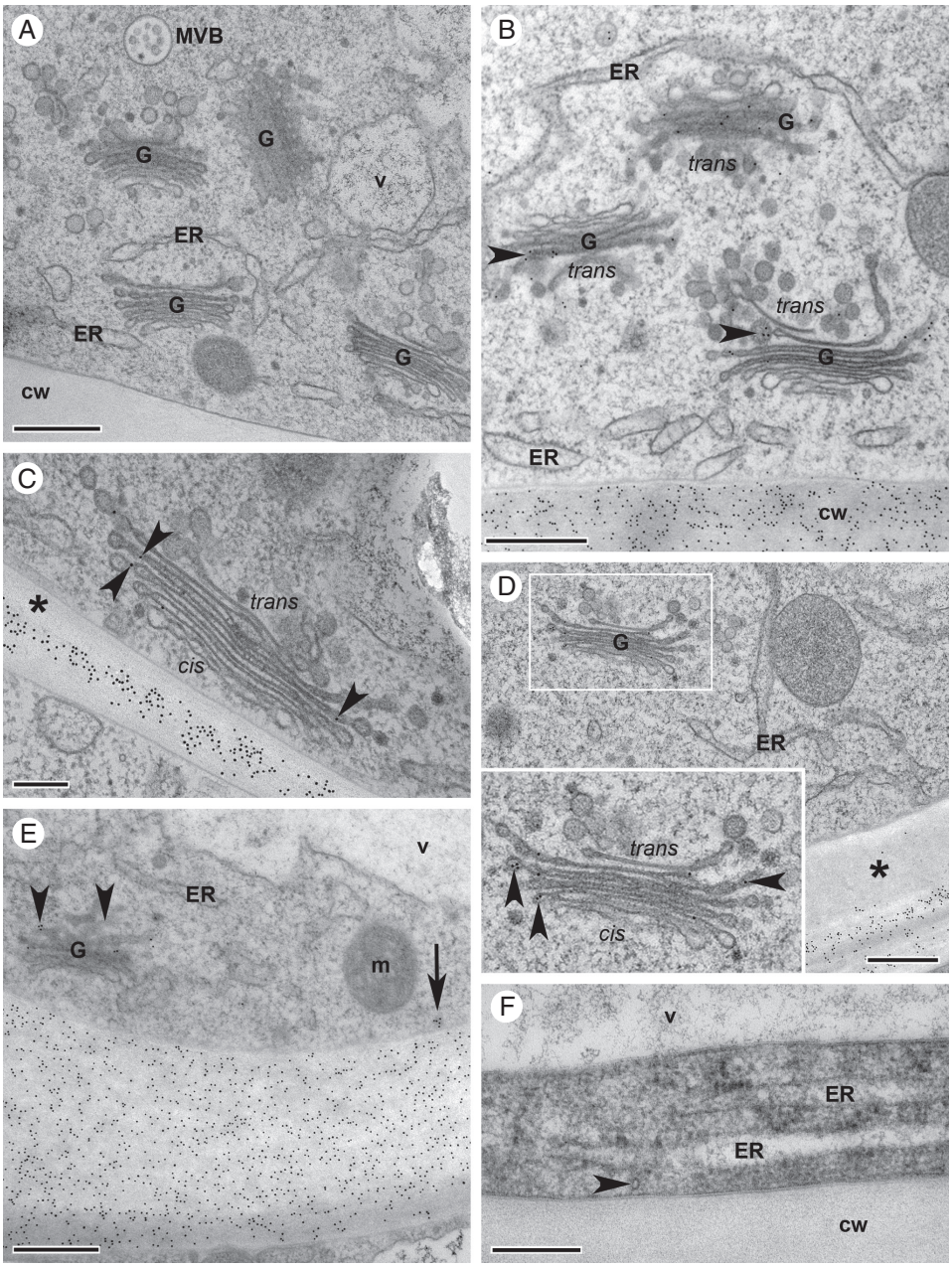

FIG. 9. Golgi stacks produce different types of pectin during asymmetric cell wall thickening in oi1 seed coat cells during stage 17 of *C. hirsuta* fruit development. Transmission electron micrographs of transverse sections of HPF-FS-processed seeds showing ultrastructural details of Golgi stacks carrying two different types of pectin in oi1 cells. (A) TEM overview depicting the abundance of Golgi stacks in oi1 cells during cell wall thickening. (B–E) Indirect immunogold labelling of JIM7 epitopes (B and E) and CCRC-M38 epitopes (C and D). Both epitopes are detected in Golgi stacks (arrowheads, B–E), commonly in the swollen margin of mid- and *trans*-located cisternae. JIM7 epitopes are distributed throughout the thickened cell wall (B and E), but CCRC-M38 epitopes are not present in newly deposited cell wall thickenings (asterisks, C and D). Inset shows the boxed region at increased magnification (D). JIM7 epitopes are detected in vesicles that can be seen fusing with or in close contact with the plasma membrane adjacent to newly deposited cell wall thickenings (arrow, E). (F) Only very rarely are microtubules found on the cytosolic side of the plasma membrane adjacent to newly deposited cell wall thickenings (arrowhead). Abbreviations: *cis*, *cis* side of the Golgi stack; cw, cell wall; ER, endoplasmic reticulum; G, Golgi stack; m, mitochondrion; MVB, multivesicular body; *trans*, *trans* side of the Golgi stack; v, vacuole. Scale bars = 500 nm (A, B, E) and 200 nm (C, D, F).

The cell wall thickenings along the inner periclinal wall of oi1 cells are strongly labelled by CCRC-M38 antibodies (Fig. 10D, E). These thickened oi1 cell walls are much more electron dense than the secondary cell walls of the columella in oi2 cells (Fig.10D, E), suggesting differential modification. However, we did not detect staining for lignin (Supplementary Data Fig. S7A, B) or suberin/cutin (Supplementary Data Fig. S7C, D) in the thickened oi1 cell walls of mature seeds.

To analyse the mature seed coat in completely dried seeds, we imbibed 1-year-old *C. hirsuta* seeds overnight in water (Fig. 10F, G). Due to water uptake and swelling of the mucilage, the outer periclinal primary cell wall of oi2 cells ruptured,

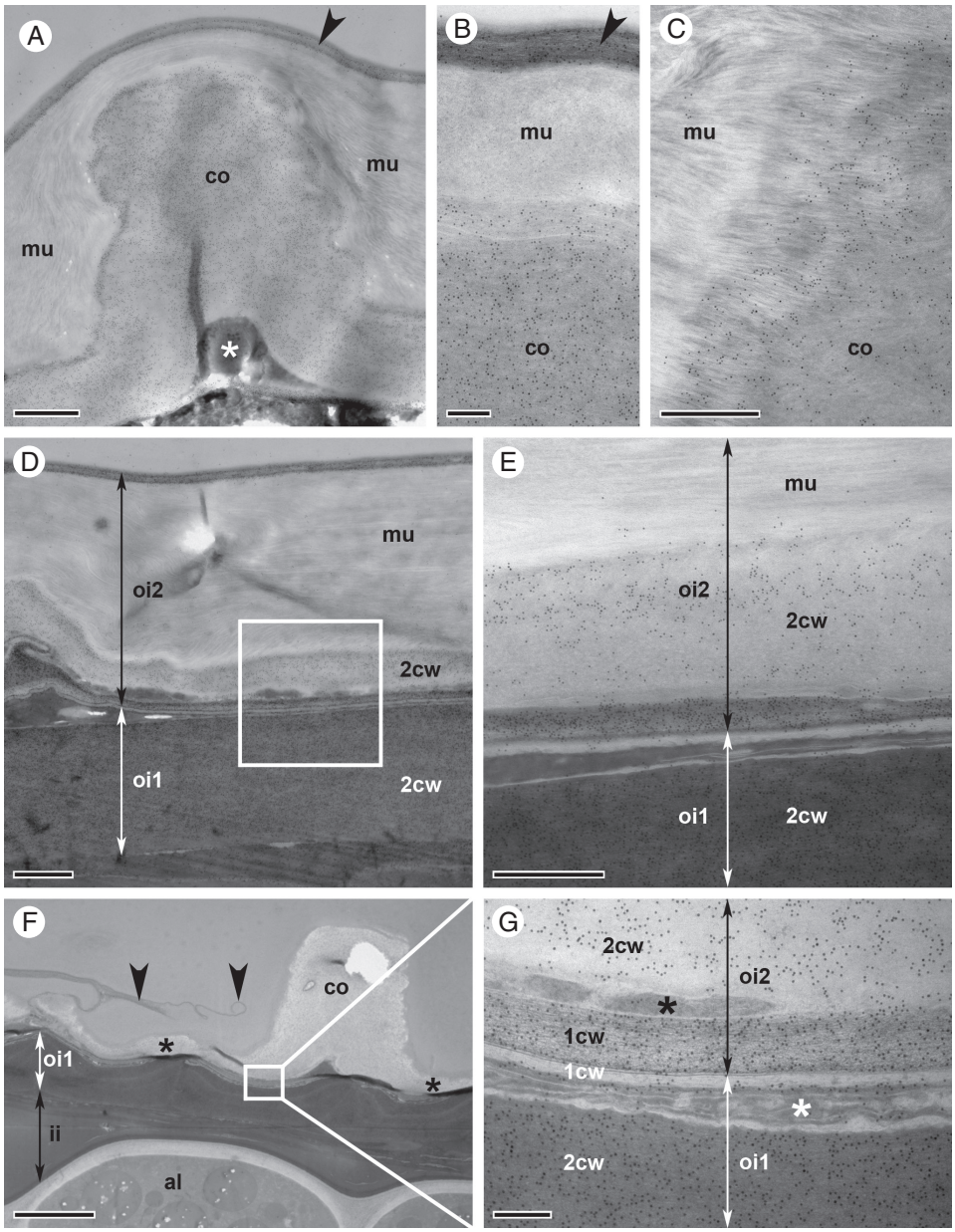

FIG. 10. Desiccated seed coat of *C. hirsuta* seeds when ejected by explosive pod shatter. Transmission electron micrographs of transverse sections of HPF-FS-processed seeds showing the distribution of CCRC-M38 epitopes in oi2 and oi1 seed coat layers. (A–E) Seeds processed without prior imbibition. The central columella of oi2 cells is covered by a layer of mucilage and the outer primary cell wall (arrowhead, A). Cytoplasmic debris is compacted to a very small space at the bottom of the columella (asterisk, A). CCRC-M38 epitopes are abundant in the columella and the outer primary oi2 cell wall (arrowhead, B) while the mucilage is not labelled (B). The border between mucilage and columella is indistinct, characterized by material with a fibrillar structure of mixed mucilage/cell wall identity (C). Overview of the layered structure of the outer seed coat made up predominantly of mucilage and oi2 and oi1 secondary cell walls (D), and higher magnification of an area similar to the boxed region (E). (F and G) Seeds processed after overnight imbibition. Overview of the seed coat with the outer primary oi2 cell wall ruptured (arrowheads, F), exposing the secondary oi2 cell wall (asterisks, F) and the columella (F). Remnants of inner seed coat layers including ii1 are located between oi1 cells and the aleurone-like layer (F). Note that oi1 cell wall thickenings and ii1 remnants are electron dense, in comparison with oi2 secondary cell walls and aleurone-like cells (F). Detail of the boxed area in (F) showing the cytoplasmic remnants of oi2 and oi1 cells (asterisks, G) squeezed by secondary cell walls produced by each cell type. Abbreviations: 1cw, primary cell wall; 2cw, secondary/thickened cell wall; al, aleurone-like layer; co, columella; ii, inner integuments; mu, mucilage; oi, outer integument. Scale bars = 1 µm (A, D), 200 nm (B, G), 500 nm (C, E) and 5 µm (F).

leaving only fragments (arrowheads, Fig. 10F). The columella, comprised entirely of secondary cell wall material, is prominently exposed at the seed surface (Fig. 10F). Immunogold labelling shows an identical structure to freshly ejected seeds, with the outer seed coat made up of alternating layers of cell wall material labelled by CCRC-M38 antibodies and crushed cytoplasmic debris of oi2 and oi1 cells (Fig. 10G). The thickened cell walls of oi1 cells and the phenolic compounds released from ii1 cells are very electron dense in comparison with cell wall material of the columella or aleurone-like layer (Fig. 10F, G). This very electron-dense area on ultrathin sections corresponds to the area delimited by suberin/cutin

layers on each side (Supplementary Data Fig. S7C, D). The innermost suberin/cutin layer, that delimits the ii1 layer of the seed coat from the aleurone-like cell layer (Supplementary Data Fig. S7D), is recognizable as an electron-dense cell wall region at the ultrastructural level as early as stage 17a of fruit development (Supplementary Data Fig. S7E). The outermost suberin/cutin layer, that delimits the oi1and oi2 layers in the seed coat (Supplementary Data Fig. S7D), becomes recognizable as an electron-dense cell wall region only at much later stages when seeds are completely desiccated (Supplementary Data Fig. S7F).

Diverse seed coat surfaces in the Brassicaceae

To investigate the association between explosive seed dispersal and structuring of the seed surface by the sub-epidermal cell layer of the seed coat, we compared the seed surface of diverse species of Brassicaceae. To our knowledge, *Cardamine* is the only genus in this large family where explosive seed dispersal is found (Hofhuis *et al*., 2016), and we observed that cell wall thickenings derived from the sub-epidermis structured the seed surface in all *Cardamine* species that we sampled (Fig. 11A, B). Furthermore, we observed that the surface of non-explosive *Arabidopsis lyrata* seeds is shaped by the columella and the anticlinal cell walls of the epidermis (Fig. 11C), similar to *A. thaliana* (Fig. 1A, B). We also observed that epidermal cell walls structured the surface of non-explosive seeds in *Leavenworthia alabamica* and *Lepidium campestre* (Fig. 11D, E). However, we found that sub-epidermal cell walls determined the seed surface in *Capsella rubella* and *Geococcus pusilus*, which employ non-explosive seed dispersal (Fig. 11F, G). Therefore, although *Cardamine* species may share both traits, explosive seed dispersal and seed surface topology derived from sub-epidermal cell walls, these traits are not associated outside of *Cardamine*. Moreover, we also found that seed surface topology varied greatly among Brassicaceae species (Vaughan and Whitehouse, 1971), from circular structures that densely cover the epidermis in *Turritus laxa* and *Aethionema arabicum* (Fig. 11H, I) and are known to extrude mucilage in *A. arabicum* (Lenser *et al*., 2016), to completely smooth epidermal cells in *Rorippa islandica* (Fig. 11J).

DISCUSSION

Form and function of the *C. hirsuta* seed coat depend on localized deposition of specialized cell walls prior to death of the seed coat cells. Differentiation of the two outermost seed coat layers involves polar deposition of distinct types of pectin produced by the Golgi apparatus. While oi2 cell differentiation is very similar between *C. hirsuta* and *A. thaliana* seeds, asymmetric deposition of a thick cell wall in sub-epidermal oi1 cells of the *C. hirsuta* seed coat produces the distinctive surface morphology of *C. hirsuta* seeds.

The explosively dispersed seeds of *C. hirsuta* are released before the fruit dries (Hofhuis *et al*., 2016), which is a much earlier developmental stage than the non-explosively dispersed seeds of *A. thaliana*. However, by comparing the seed coat of freshly ejected *C. hirsuta* seeds with that of dried seeds, we found no differences (Fig. 10), suggesting that the seed coat is fully mature in these explosively dispersed seeds.

Cardamine hirsuta seeds are also larger than *A. thaliana* seeds (Hay *et al*., 2014). In *A. thaliana*, the timing of endosperm cellularization during seed development is a key determinant of final seed size (Scott *et al*., 1998; Garcia *et al*., 2003). Endosperm cellularization first starts in *A. thaliana* seeds with early heart-stage embryos (5 d after pollination; Batista *et al*., 2019) and is complete in all but the chalazal chamber when embryos reach the torpedo stage (7 d after pollination; Mansfield and Briarty, 1990; Brown *et al*., 1999; Batista *et al*., 2019). In comparison, endosperm cellularization is first observed in *C. hirsuta* seeds with late heart-stage embryos (Supplementary Data Fig. S3B), and most of the endosperm is still not cellularized in seeds with torpedo-stage embryos (Fig. 3E; Supplementary Data Fig. S3C–E). Therefore, the timing of endosperm cellularization appears to differ between *C. hirsuta* and *A. thaliana*, with later cellularization associated with larger seed size in *C. hirsuta*.

During seed coat development in *C. hirsuta*, large amounts of pectic polysaccharides are secreted to localized regions of the cell wall in epidermal oi2 cells and sub-epidermal oi1 cells (Fig. 12). Prior to pectin secretion, oi2 and oi1 cells accumulate amyloplasts containing large starch granules, which may provide the primary source of carbon for pectin synthesis (Fig. 12A). However, the starchless *phosphoglucomutase 1* mutant in *A. thaliana* was still able to produce mucilage in epidermal oi2 cells (Western *et al*., 2000), suggesting that this hypothesis requires further investigation. Oi2 cells secrete mucilage, which contains RGI-rich pectin, into a ring-shaped pocket between the outer periclinal cell wall and the plasma membrane (Fig. 12A). Following mucilage secretion, the epidermal cells synthesize a thick, cellulosic secondary cell wall containing HG pectin across the apical surface of the column-shaped cytoplasm. This columella protrudes through the centre of the mucilage pocket at seed maturity (Fig. 12B). HG pectins are also abundant in the thick cell wall deposited on the inner periclinal surface of oi1 cells and part way up the adjacent anticlinal walls (Fig. 12A). These thickened cell walls form prominent ridges on the surface of mature *C. hirsuta* seeds (Fig. 12B).

Striking changes in the number and appearance of Golgi stacks are associated with the polar secretion of pectic polysaccharides in oi2 and oi1 cells of the *C. hirsuta* seed coat (Fig. 12A). Golgi stacks increase in number and complexity, with the attached TGN forming extended, interconnected tubes which, in cross-view on ultrathin sections, can be misinterpreted as large secretory vesicles. Within the Golgi stack, CCRC-M38 and JIM7 epitopes were most abundant in the swollen margins of mid- and *trans*-located cisternae and not detected in the TGN (Fig. 9). These antibodies preferentially recognize HG pectins with a high degree of methyl esterification (JIM7; Knox *et al*., 1990) and a low degree of methyl esterification (CCRC-M38; Pattathil *et al*., 2010). Therefore, in line with previous studies (Zhang and Staehelin, 1992), our results suggest that de-esterified HG pectin, recognized by CCRC-M38, is synthesized and subsequently modified in the Golgi to produce methyl esterified HG pectin,

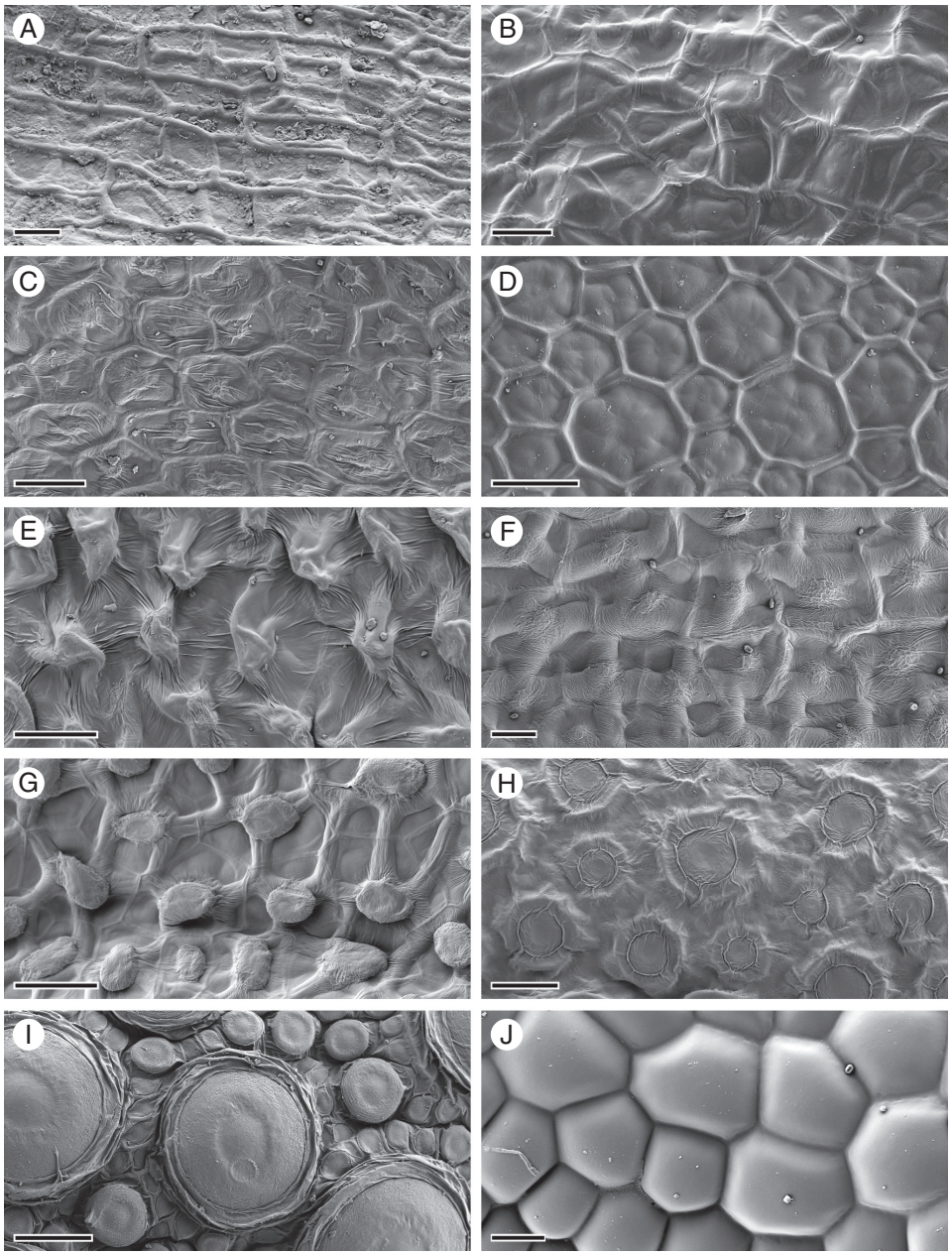

Fig. 11. Seed coat diversity in the Brassicaceae. (A) *Cardamine trifolia*. (B) *Cardamine corymbosa*. (C) *Arabidopsis lyrata*. (D) *Leavenworthia alabamica*. (E) *Lepidium campestre*. (F) *Capsella rubella*. (G) *Geococcus pusilus*. (H) *Turritus laxa*. (I) *Aethionema arabicum*. (J) *Rorippa islandica*. Scale bars = 20 µm (A–C, F, J) and 50 µm (D, E, G–I).

recognized by JIM7 (Fig. 12A). We also detected this methyl esterified form of HG pectin in vesicles fusing, or in close contact, with the plasma membrane adjacent to asymmetric cell wall thickenings in oi1 cells (Fig. 9E). Therefore, methyl esterified HG pectin is secreted to these specific regions of the plasma membrane via vesicles that probably bud off from Golgi cisternae proximal to the TGN (Fig. 12A).

Highly methyl esterified pectin was previously detected in the asymmetrically thickened cell walls of *C. hirsuta* oi1 cells by LM20 antibody labelling (Gan *et al*., 2016). Our current results extend this finding to show that although HG pectin is secreted and uniformly distributed throughout the cell wall in a methyl esterified form, recognized by JIM7, de-esterified HG pectin is also detected by CCRC-M38 labelling (Figs 8 and 9). Given that CCRC-M38 labelling forms a gradient that decreases towards the newly deposited cell wall thickenings, adjacent to the plasma membrane (Figs 8F, G and 9C, D), we propose that PMEs hydrolyse the methyl esters from HG pectin in older parts of the thickened cell wall (Chebli and Geitmann, 2017) (Fig. 12A).

Immunolabelling studies with the CCRC-M36 antibody in *A. thaliana* oi2 cells indicate that RGI pectin is synthesized in Golgi dispersed throughout the cell and delivered specifically to the plasma membrane domain adjacent to the mucilage pocket

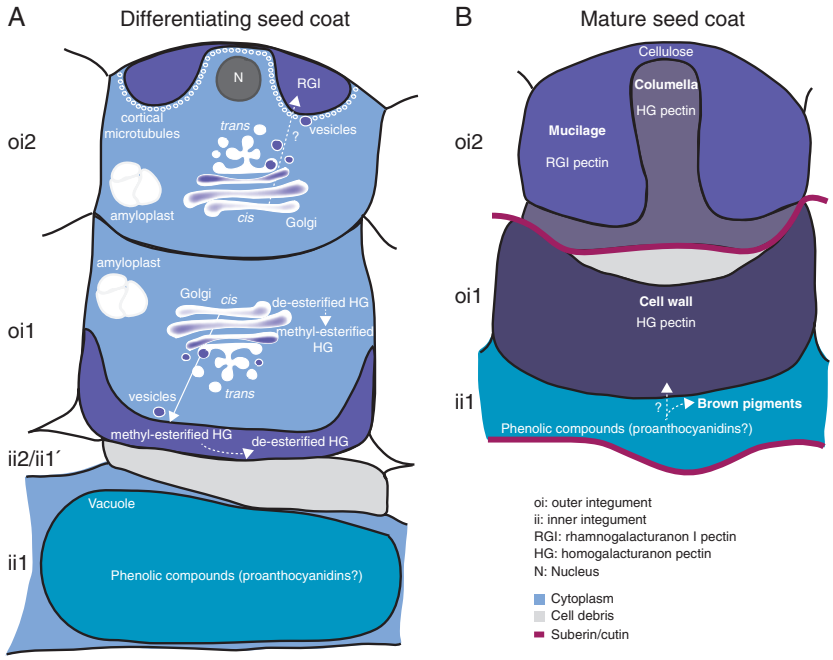

FIG. 12. Overview of seed coat differentiation in *C. hirsuta*. Three cell layers (oi2, oi1 and ii1) of ovule integuments differentiate to form the mature seed coat. (A) In oi2 cells, RGI pectin is detected in a ring-shaped pocket between the primary cell wall and the plasma membrane. The nucleus is located in the centre of this ring, close to the outer wall. Cortical microtubules line the plasma membrane adjacent to the mucilage pocket. A large number of Golgi stacks are distributed throughout oi2 cells. We propose that RGI pectin is synthesized in the Golgi and secreted via vesicles to the mucilage pocket (dashed arrow). Numerous amyloplasts containing large starch granules are produced and degraded during mucilage production in oi2 cells and cell wall thickening in oi1 cells. HG pectin is synthesized and methyl esterified in the large number of Golgi stacks distributed throughout oi1 cells. Highly methyl esterified HG pectin is secreted to the inner periclinal cell wall and part way up the adjacent anticlinal walls. Pectin de-esterification occurs in the cell wall such that HG pectin with both high and low degrees of methyl esterification is detected as cell wall thickening continues. Inner integument layers ii2 and ii1' are crushed during seed coat differentiation. Large vacuoles in ii1 cells accumulate phenolic compounds that we propose may correspond to proanthocyanidins. (B) All three cell layers are dead in the mature seed coat. Dessicated oi2 cells comprise mucilage, surrounding a columella. The secondary cell wall of the columella contains HG pectin, whereas mucilage does not. Cellulose accumulates in adherent mucilage at the top of the columella. The thickened inner periclinal cell wall of oi1 cells contains HG pectin. Phenolic compounds released from ii1 cells may correspond to proanthocyanidins, which can be oxidized to brown pigments. Oxidation and polymerization of these phenolic compounds may also occur in thickened oi1 cell walls (dashed arrow). Two suberin/cutin layers delimit the ii1 and oi1 cell layers and may prevent diffusion of phenolic compounds beyond these layers.

(McFarlane *et al*., 2008; Young *et al*., 2008). Although RGI pectin was labelled by CCRC-M36 in the mucilage pockets of *C. hirsuta* oi2 cells (Fig. 5), this signal could not be detected by TEM – probably because recognition of the CCRC-M36 epitope was altered by the presence of osmium in these experiments. However, given the similarities in oi2 cell ultrastructure between *C. hirsuta* and *A. thaliana* during mucilage production, it is likely that RGI pectin is synthesized and secreted to the mucilage pocket of *C. hirsuta* oi2 cells in a similar manner (Fig. 12A).

The polar secretion of different pectins to specific regions of the plasma membrane in *C. hirsuta* oi2 and oi1 cells is associated with Golgi stacks that are dispersed throughout the cell rather than concentrated near the site of cargo deposition (Figs 7 and 9). This suggests that pectin secretion is likely to occur via a post-Golgi targeting mechanism in both cell types. In oi2 cells, cortical microtubules specifically accumulate in close vicinity to the plasma membrane in regions where mucilage secretion occurs (Fig. 12A). Previous work suggested that microtubules may be involved in polar mucilage secretion in *A. thaliana* oi2 cells; however, it was unclear whether the cargo of the small, electron-dense vesicles in close association with microtubules included pectin (McFarlane *et al*., 2008). Another function of cortical microtubules is to position the delivery of cellulose synthase (CESA) complexes to the plasma membrane and guide the trajectories of active CESA complexes (Paredez *et al*., 2006; Gutierrez *et al*., 2009). Therefore, cortical microtubules that line the mucilage secretion domain in *C. hirsuta* oi2 cells may contribute to cellulose synthesis in the secondary cell wall of the columella (Supplementary Data Fig. S1). The dense array of cortical microtubules along the apical domain of the cytoplasmic column (Fig. 7H) also correlates with cellulose that is present above the columella in adherent mucilage, and extends in a spiral pattern upon water imbibition (Supplementary Data Fig. S1; Fig. 12B) (Macquet *et al*., 2007; Ralet *et al*., 2016). Disrupting microtubules by depolymerization or genetic perturbations should help ascribe function to the cortical arrays observed in oi2 seed coat cells. However, disrupting microtubule organization in the *microtubule organisation1* mutant was not sufficient to affect mucilage secretion or columella formation in *A. thaliana* (McFarlane *et al*., 2008), suggesting that these questions are not straightforward to address.

The asymmetric cell wall thickenings in oi1 cells of the *C. hirsuta* seed coat are somewhat atypical of secondary cell walls. For instance, the cellulosic wall is deposited asymmetrically in the cell after expansion has finished, but it is pectin rich, contains xyloglucans and is not lignified or suberized (Fig. 5; Supplementary Data Fig. S7) (Cosgrove, 2018; Meents *et al*.,

2018). Cortical microtubules, which often line the plasma membrane and guide cellulose deposition at regions of secondary cell wall formation (Watanabe *et al*., 2015), were only rarely detected adjacent to oi1 cell wall thickenings by TEM (Fig. 9). However, it is possible that these pectin-rich oi1 cell wall thickenings may be reinforced by the oxidation and cross-linking of phenolic compounds released by the adjacent ii1 layer during seed desiccation (Fig. 12B). Phenolic compounds fill the large vacuoles that almost completely occupy cells of the inner integument (ii1) during *C. hirsuta* seed coat development (Figs 3 and 12A). At seed desiccation, these phenolic compounds, together with the dead and crushed cells of the inner integument, form an electron-dense layer directly beneath the thick oi1 cell walls (Figs 10F and 12B). Oi1 cell walls have a similar electron density to the ii1 remnants (Fig. 10), suggesting that phenolic compounds liberated from ii1 may also impregnate the thickened cell wall in oi1 cells. The presence of suberin/cutin between oi1 and oi2 cell layers, and between the seed coat and the aleurone-like cell layer, may act as barriers to prevent further diffusion of these phenolic compounds (Supplementary Data Fig. S7C–F; Fig. 12B).

Proanthocyanidins are phenolic compounds that accumulate exclusively in ii1 cells of the *A. thaliana* seed coat and, upon cell death, form oxidized complexes with cell wall polysaccharides (Debeaujon *et al*., 2003; Pourcel *et al*., 2005). This process causes brown pigmentation, which is observed in *C. hirsuta* seeds from stage 16 of fruit development onwards (Supplementary Data Fig. S2). *LAC15* (*TT10*, At5g48100) encodes a laccase oxidase, and its gene expression co-localizes first with proanthocyanidin-producing ii1 cells and then with flavonol-producing oi1 cells during development of the *A. thaliana* seed coat (Pourcel *et al*., 2005). During seed desiccation, the oxidation of flavonoids by LAC15 might increase their capacity to bind to the cell wall and strengthen the seed coat (Pourcel *et al*., 2005). By analogy, a similar flavonoid oxidase may function in the *C. hirsuta* seed coat to form flavonoid derivatives that strengthen the pectin-rich cell wall thickenings in oi1 cells (Fig. 12B).

We found that the differential contribution of cell walls derived from oi2 vs. oi1 cells to the topography of *A. thaliana* vs. *C. hirsuta* seeds extends to other species within *Arabidopsis* and *Cardamine*. For example, non-explosive *A. thaliana* and *A. lyrata* seeds look alike, as do explosive *C. hirsuta* and *C. corymbosa* seeds (Fig. 11). So, it is interesting to speculate how a ridged seed surface could influence explosive seed dispersal in *Cardamine* species. At very low Reynolds numbers these ridges are unlikely to act as turbulators, like dimples on a golf ball, to reduce aerodynamic drag. However, a ridged seed surface may influence seed launch or flight in other ways that affect dispersal. For example, the explosively dispersed seeds of *Ruellia ciliatiflora* are launched with stabilizing backspin in an orientation that minimizes drag, thereby increasing dispersal range (Cooper *et al*., 2018; Seale and Nakayama, 2019). Therefore, these questions warrant further investigation in *C. hirsuta*. Importantly, we found that other Brassicaceae species with non-explosive seed dispersal had diverse seed coat morphologies, contributed by both epidermal and sub-epidermal seed coat layers (Fig. 11). So, while it is possible that the surface structure of *Cardamine* seeds may aid seed launch or ballistic flight, this characteristic of the seed coat did not coevolve with explosive seed dispersal.

SUPPLEMENTARY DATA

Supplementary data are available online at https://academic.oup.com/aob and consist of the following.

Figure S1: mucilage extrusion from *C. hirsuta* oi2 cells upon chemical fixation in aqueous fixatives.

Figure S2: seed coat pigmentation.

Figure S3: early stages of embryo development.

Figure S4: indirect immunogold labelling of oi2 seed coat cells by CCRC-M36 antibodies at the peak of mucilage secretion.

Figure S5: ultrastructural features of oi2 cells during mucilage secretion.

Figure S6: oi2 cells possess complex lipid-containing vacuoles.

Figure S7: lignin and suberin are absent from thickened oi1 cell walls.

FUNDING

This work was supported by a Minerva Fellowship from the Max Planck Society to A.H.

ACKNOWLEDGEMENTS

We thank C. Hawes and M. Tsiantis for useful discussions and comments on the manuscript, and dedicate this work to the memory of C. Hawes who recently passed away. We thank I. Rouhara for transmission electron microscopy sample preparation, R. Franzen for scanning electron microscopy, H. Dickinson and L. Nikolov for sharing Brassicaceae seeds, and P. Huijser for DIC image processing and help with confocal imaging.

LITERATURE CITED

Batista RA, Figueiredo DD, Santos-Gonzalez J, Kohler C. 2019. Auxin regulates endosperm cellularization in *Arabidopsis*. *Genes and Development* **33**: 466–476.

Beeckman T, De Rycke R, Viane R, Inze D. 2000. Histological study of seed coat development in *Arabidopsis thaliana*. *Journal of Plant Research* **113**: 139–148.

Blake AW, McCartney L, Flint JE, *et al.* 2006. Understanding the biological rationale for the diversity of cellulose-directed carbohydrate-binding modules in prokaryotic enzymes. *Journal of Biological Chemistry* **281**: 29321–29329.

Brown RC, Lemmon BE, Nguyen H, Olsen OA. 1999. Development of endosperm in *Arabidopsis thaliana*. *Sexual Plant Reproduction* **12**: 32–42.

Chebli Y, Geitmann A. 2017. Cellular growth in plants requires regulation of cell wall biochemistry. *Current Opinion in Cell Biology* **44**: 28–35.

Cooper ES, Mosher MA, Cross CM, Whitaker DL. 2018. Gyroscopic stabilization minimizes drag on *Ruellia ciliatiflora* seeds. *Journal of the Royal Society, Interface* **15**: pii: 20170901. doi: 10.1098/rsif.2017.0901.

Cosgrove DJ. 2016. Catalysts of plant cell wall loosening. *F1000Research* **5**: pii: F1000 Faculty Rev-119. doi: 10.12688/f1000research.7180.1.

Cosgrove DJ. 2018. Primary walls in second place. *Nature Plants* **4**: 748–749.

Creff A, Brocard L, Ingram G. 2015. A mechanically sensitive cell layer regulates the physical properties of the *Arabidopsis* seed coat. *Nature Communications* **6**: 6382. doi: 10.1038/ncomms7382.

Debeaujon I, Nesi N, Perez P, *et al.* 2003. Proanthocyanidin-accumulating cells in *Arabidopsis* testa: regulation of differentiation and role in seed development. *The Plant Cell* **15**: 2514–2531.

Dinneny JR, Yanofsky MF. 2005. Drawing lines and borders: how the dehiscent fruit of *Arabidopsis* is patterned. *Bioessays* **27**: 42–49.

Donohoe BS, Kang BH, Staehelin LA. 2007. Identification and characterization of COPIa- and COPIb-type vesicle classes associated with plant and algal Golgi. *Proceedings of the National Academy of Sciences, USA* **104**: 163–168.

Fuchs C. 1963. Fuchsin staining with NaOH clearing for lignified elements of whole plants of plants organs. *Stain Technology* **38**: 141–144.

Galstyan A, Hay A. 2018. Snap, crack and pop of explosive fruit. *Current Opinion in Genetics & Development* **51**: 31–36.

Gan X, Hay A, Kwantes M, *et al.* 2016. The *Cardamine hirsuta* genome offers insight into the evolution of morphological diversity. *Nature Plants* **2**: 16167. doi: 10.1038/nplants.2016.167.

Garcia D, Saingery V, Chambrier P, Mayer U, Jurgens G, Berger F. 2003. Arabidopsis *haiku* mutants reveal new controls of seed size by endosperm. *Plant Physiology* **131**: 1661–1670.

Gutierrez R, Lindeboom JJ, Paredez AR, Emons AM, Ehrhardt DW. 2009. *Arabidopsis* cortical microtubules position cellulose synthase delivery to the plasma membrane and interact with cellulose synthase trafficking compartments. *Nature Cell Biology* **11**: 797–806.

Haughn G, Chaudhury A. 2005. Genetic analysis of seed coat development in *Arabidopsis*. *Trends in Plant Science*, **10**: 472–477.

Haughn GW, Western TL. 2012. *Arabidopsis* seed coat mucilage is a specialized cell wall that can be used as a model for genetic analysis of plant cell wall structure and function. *Frontiers in Plant Science* **3**: 64. doi: 10.3389/fpls.2012.00064.

Hay A, Tsiantis M. 2006. The genetic basis for differences in leaf form between *Arabidopsis thaliana* and its wild relative *Cardamine hirsuta*. *Nature Genetics* **38**: 942–947.

Hay A, Tsiantis M. 2016. *Cardamine hirsuta*: a comparative view. *Current Opinion in Genetics & Development* **39**: 1–7.

Hay AS, Pieper B, Cooke E, *et al.* 2014. *Cardamine hirsuta*: a versatile genetic system for comparative studies. *The Plant Journal* **78**: 1–15.

Hayashi M, Gerry SP, Ellerby DJ. 2010. The seed dispersal catapult of *Cardamine parviflora* (Brassicaceae) is efficient but unreliable. *American Journal of Botany* **97**: 1595–1601.

Hofhuis H, Moulton D, Lessinnes T, *et al.* 2016. Morphomechanical innovation drives explosive seed dispersal. *Cell* **166**: 222–233.

Knox JP, Linstead PJ, King J, Cooper C, Roberts K. 1990. Pectin esterification is spatially regulated both within cell walls and between developing tissues of root apices. *Planta* **181**: 512–521.

Lenser T, Graeber K, Cevik ZS, *et al.* 2016. Developmental control and plasticity of fruit and seed dimorphism in *Aethionema arabicum*. *Plant Physiology* **172**: 1691–1707.

Lepiniec L, Debeaujon I, Routaboul JM, *et al.* 2006. Genetics and biochemistry of seed flavonoids. *Annual Review of Plant Biology* **57**: 405–430.

Macquet A, Ralet MC, Kronenberger J, Marion-Poll A, North HM. 2007. In situ, chemical and macromolecular study of the composition of *Arabidopsis thaliana* seed coat mucilage. *Plant & Cell Physiology* **48**: 984–999.

Mansfield SG, Briarty LG. 1990. Endosperm cellularization in *Arabidopsis thaliana* L. *Arabidopsis Information Service* **27**: 65–72.

McCartney L, Gilbert HJ, Bolam DN, Boraston AB, Knox JP. 2004. Glycoside hydrolase carbohydrate-binding modules as molecular probes for the analysis of plant cell wall polymers. *Anals of Biochemistry* **326**: 49–54.

McDonald KL. 2014. Rapid embedding methods into epoxy and LR White resins for morphological and immunological analysis of cryofixed biological specimens. *Microscopy and Microanalysis* **20**: 152–163.

McFarlane HE, Young RE, Wasteneys GO, Samuels AL. 2008. Cortical microtubules mark the mucilage secretion domain of the plasma membrane in *Arabidopsis* seed coat cells. *Planta* **227**: 1363–1375.

Meents MJ, Watanabe Y, Samuels AL. 2018. The cell biology of secondary cell wall biosynthesis. *Annals of Botany* **121**: 1107–1125.

Micali CO, Neumann U, Grunewald D, Panstruga R, O'Connell R. 2011. Biogenesis of a specialized plant–fungal interface during host cell internalization of *Golovinomyces orontii haustoria*. *Cell Microbiology* **13**: 210–226.

Moran DT, Rowley JC. 1988. *Visual histology*. Philadelphia, PA: Lea & Febiger.

Mori B, Bellani LM. 1996. Differential staining for cellulosic and modified plant cell walls. *Biotechnic & Histochemistry* **71**: 71–72.

Musielak TJ, Slane D, Liebig C, Bayer M. 2016. A versatile optical clearing protocol for deep tissue imaging of fluorescent proteins in *Arabidopsis thaliana. PLoS One* **11**: e0161107. doi: 10.1371/journal.pone.0161107.

North H, Baud S, Debeaujon I, *et al.* 2010. *Arabidopsis* seed secrets unravelled after a decade of genetic and omics-driven research. *The Plant Journal* **61**: 971–981.

O'Brien TP, Feder N, McCully ME. 1964. Polychromatic staining of plant cell walls by toluidine blue O. *Protoplasma* **59**: 367–373.

Pain C, Kriechbaumer V, Kittelmann M, Hawes C, Fricker M. 2019. Quantitative analysis of plant ER architecture and dynamics. *Nature Communications* **10**: 984. doi: 10.1038/s41467-019-08893-9.

Paredez AR, Somerville CR, Ehrhardt DW. 2006. Visualization of cellulose synthase demonstrates functional association with microtubules. *Science* **312**: 1491–1495.

Pattathil S, Avci U, Baldwin D, *et al.* 2010. A comprehensive toolkit of plant cell wall glycan-directed monoclonal antibodies. *Plant Physiology* **153**: 514–525.

Pedersen HL, Fangel JU, McCleary B, *et al.* 2012. Versatile high resolution oligosaccharide microarrays for plant glycobiology and cell wall research. *Journal of Biological Chemistry* **287**: 39429–39438.

Pourcel L, Routaboul JM, Kerhoas L, Caboche M, Lepiniec L, Debeaujon I. 2005. TRANSPARENT TESTA10 encodes a laccase-like enzyme involved in oxidative polymerization of flavonoids in *Arabidopsis* seed coat. *The Plant Cell* **17**: 2966–2980.

Ralet MC, Crepeau MJ, Vigouroux J, *et al.* 2016. Xylans provide the structural driving force for mucilage adhesion to the *Arabidopsis* seed coat. *Plant Physiology* **171**: 165–178.

Reynolds ES. 1963. The use of lead citrate at high pH as an electron-opaque stain in electron microscopy. *Journal of Cell Biology* **17**: 208–212.

Robinson DG, Brandizzi F, Hawes C, Nakano A. 2015. Vesicles versus tubes: is endoplasmic reticulum–Golgi transport in plants fundamentally different from other eukaryotes? *Plant Physiology* **168**: 393–406.

Robinson DG, Pimpl P. 2014. Clathrin and post-Golgi trafficking: a very complicated issue. *Trends in Plant Science* **19**: 134–139.

Roeder AH, Yanofsky MF. 2006. Fruit development in *Arabidopsis*. *The Arabidopsis Book* **4**: e0075. doi: 10.1199/tab.0075.

Scott RJ, Spielman M, Bailey J, Dickinson HG. 1998. Parent-of-origin effects on seed development in *Arabidopsis thaliana*. *Development* **125**: 3329–3341.

Seale M, Nakayama N. 2019. From passive to informed: mechanical mechanisms of seed dispersal. *New Phytologist* doi: https://doi.org/10.1111/nph.16110

Spence J. 2001. Plant histology. In: Hawes C, Satiat-Jeunemaitre B, eds. *Plant cell biology: a practical approach*. Oxford: Oxford University Press, 189–206.

Swaine MD, Beer T. 1977. Explosive seed dispersal in *Hura crepitans* L (Euphorbiaceae). *New Phytologist*, **78**: 695–708.

Ursache R, Andersen TG, Marhavy P, Geldner N. 2018. A protocol for combining fluorescent proteins with histological stains for diverse cell wall components. *The Plant Journal*, **93**: 399–412.

Vaughan JG, Whitehouse JM. 1971. Seed structure and taxonomy of Cruciferae. *Botanical Journal of the Linnean Society* **64**: 383–409.

Vaughn KC, Bowling AJ, Ruel KJ. 2011. The mechanism for explosive seed dispersal in *Cardamine hirsuta* (Brassicaceae). *American Journal of Botany* **98**: 1276–1285.

Vogel S. 2005. Living in a physical world – II. The bio-ballistics of small projectiles. *Journal of Biosciences* **30**: 167–175.

Watanabe Y, Meents MJ, McDonnell LM, *et al.* 2015. Visualization of cellulose synthases in *Arabidopsis* secondary cell walls. *Science* **350**: 198–203.

Western TL, Skinner DJ, Haughn GW. 2000. Differentiation of mucilage secretory cells of the *Arabidopsis* seed coat. *Plant Physiology* **122**: 345–356.

Wilson SM, Ho YY, Lampugnani ER, *et al.* 2015. Determining the subcellular location of synthesis and assembly of the cell wall polysaccharide (1,3;1,4)-beta-D-glucan in grasses. *The Plant Cell* **27**: 754–771.

Young RE, McFarlane HE, Hahn MG, Western TL, Haughn GW, Samuels AL. 2008. Analysis of the Golgi apparatus in *Arabidopsis* seed coat cells during polarized secretion of pectin-rich mucilage. *The Plant Cell* **20**: 1623–1638.

Zhang GF, Staehelin LA. 1992. Functional compartmentation of the Golgi apparatus of plant cells: immunocytochemical analysis of high-pressure frozen- and freeze-substituted sycamore maple suspension culture cells. *Plant Physiology* **99**: 1070–183.